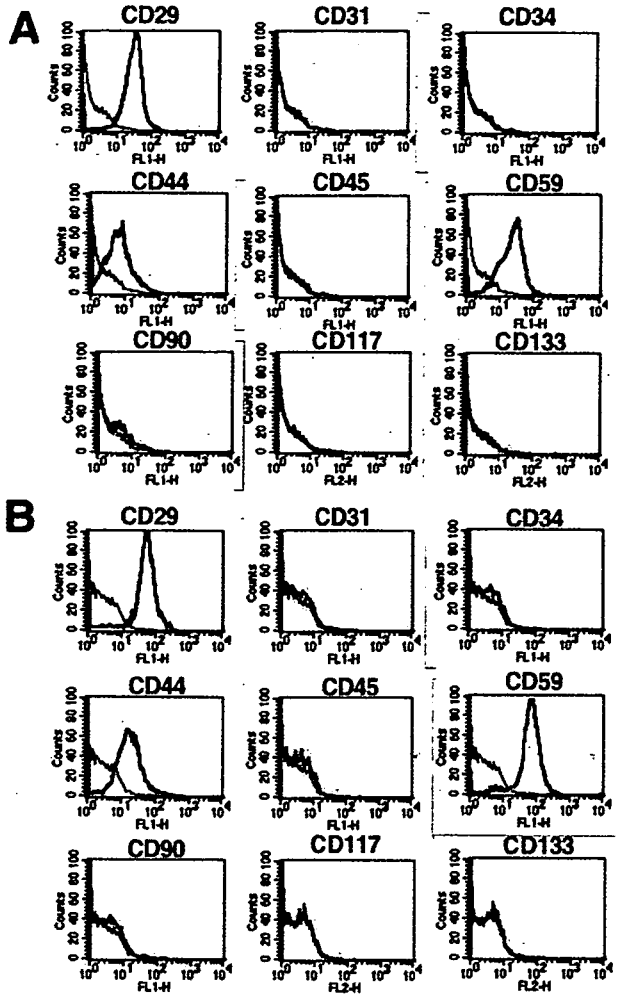

C

Surface marker	UCBMSCs	UCBTERT-21
CD34	-	-
CD117	-	-
CD31	-	-
CD13	-	-
CD14	-	-
CD29	+++	+++
CD44	++	++
CD45	-	-
CD50	-	-
CD55	++	++
CD59	+++	+++
CD90	-	-
CD133	-	-

Figure 2. Flow cytometric analysis of cell surface markers of UCBMSCs and UCBTERT-21 cells. UCBMSCs (A) displayed the same pattern of surface markers as UCBTERT-21 cells (B). No difference in cell surface markers was found between UCBMSCs and UCBTERT-21 cells as summarized in the table (C). Both were positive for CD29 (integrin β1), CD44 (Pgp-1/ly-24), and CD59, and negative for CD31 (PECAM-1), CD34, CD45 (leukocyte common antigen), CD90 (Thy-1), CD117 (c-kit), and CD133.

gal activity enzyme cytochemically at PD 32 (Figure 1D, right column).

The cells did not undergo malignant transformation. They stopped dividing after reaching confluence, and they did not form any foci after confluence in vitro. Nor did the cells grafted into the subcutaneous and muscle tissue of nude mice (n = 6) produce tumors, at least during the monitoring period (>100 d). Injected UCBTERT-21 cells survived but did not proliferate at the injection sites.

Unchanged Surface Markers of UCBMSCs after Prolongation of Their Life Span

Expression of UCBMSCs and UCBTERT-21 cell surface markers was evaluated by flow cytometric analysis (Figure 2). The results showed that both cells were positive for CD29 (integrin β1), CD44 (Pgp-1/ly-24), CD55, and CD59, and negative for CD13, CD14 (a marker for macrophages and dendritic cells), CD31 (platelet-endothelial cell adhesion molecule-1, PECAM-1), CD34, CD45 (leukocyte common antigen), CD50 (intercellular adhesion molecule-1, ICAM-1), CD90 (Thy-1), CD117 (c-kit), and CD133. Primary UCBMSCs displayed the same pattern of surface markers as UCBTERT-21 cells, implying that the surface marker expression was unaffected by the exogenously expressed hTERT.

Absence of $p16^{INK4a}$ in Parental UCBMSCs

Expression of $p16^{INK4a}$/RB premature senescence-associated proteins (Figure 3A) and telomere/p53 replicative senescence-associated proteins (Figure 3B) was analyzed in UCBMSCs, UCBTERT-21, and UCBE6E7-20 cells. $p16^{INK4a}$ was not detected in the UCBMSC lanes until the senescence stage; $p16^{INK4a}$ was not detected until PD 53 and started to be expressed in UCBTERT-21 cells at a low level at PD 69, and $p16^{INK4a}$ was detected in UCBE6E7-20 cells at PD 37, immediately before the crisis stage. The protein levels of p53 and p21 in UCBMSCs became up-regulated as the number of PDs increased, but the protein levels of p53 and p21 became down-regulated in UCBE6E7-20 cells, implying that exogenously introduced E6 targets p53 for proteolytic degradation. ATM in UCBE6E7-20 cells was phosphorylated, probably because of DNA damage or telomere length shortening (Figure 3B, lane 8). p53, phosphorylated p53, and p21 were induced by H_2O_2, a physiological stressor, in UCBTERT-21 cells (Figure 3B, lane 9). The hypophosphorylated forms of

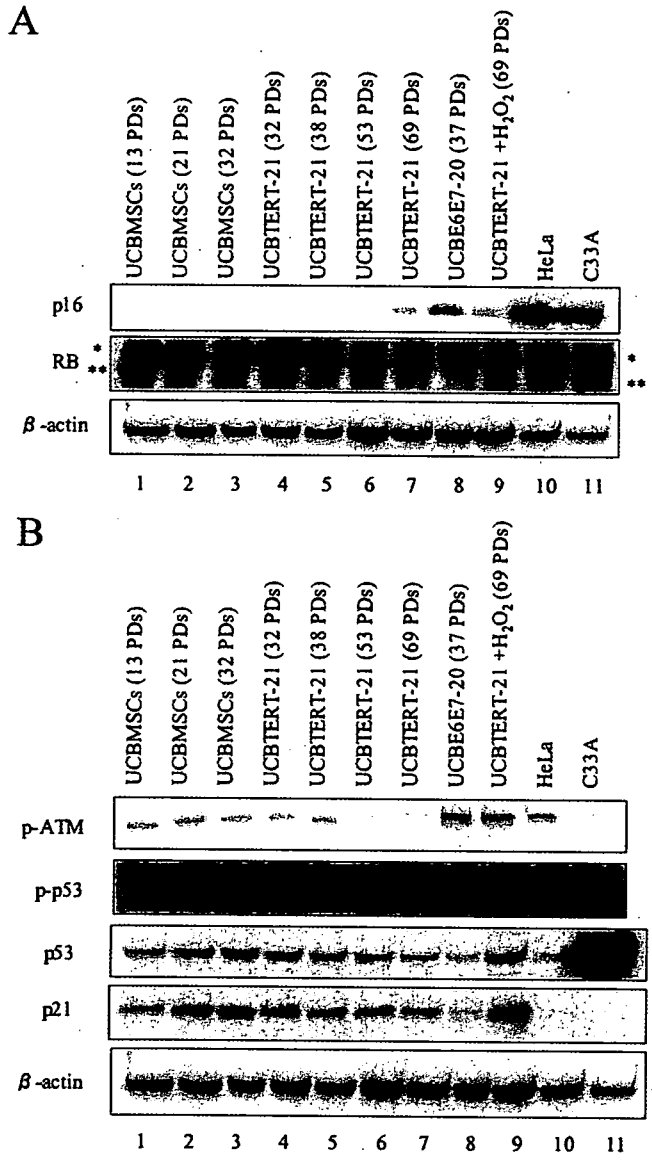

Figure 3. Time-course analysis of cell cycle-associated protein levels in UCBMSCs, UCBE6E7-20 cells, and UCBTERT-21 cells. UCBMSCs, UCBE6E7-20 cells, and UCBTERT-21 cells were analyzed by Western blotting for cell cycle-associated $p16^{INK4a}$, RB, p-ATM (Ser1981), phospho-p53 (p-p53) (Ser15), p53, p21 and β-actin protein levels. (A) "$p16^{INK4a}$-RB" senescence (premature senescence) pathway-associated protein levels, i.e., $p16^{INK4a}$ and RB. The hyperphosphorylated and hypophosphorylated forms of RB were indicated as a single asterisk and double asterisks, respectively. (B) Telomere shorten-p53' senescence (replicative senescence) pathway-associated protein levels, i.e., p-ATM, p-p53, p53, and p21. Cells were cultured for the PDs indicated and assayed. Expression of β-actin protein was monitored as a loading control.

RB became dominant and the hyperphosphorylated forms decreased with passage of UCBMSCs (Figure 3A, lanes 1–3), correlating to the increase in p53 and p21 (Figure 3B, lanes 1–3) and to the decrease in cell growth. Transduction of hTERT transiently and markedly increased the hyperphosphorylated form (Figure 3A, lane 4), corresponding to the sudden recovery in proliferation and to a shorter doubling time. Finally, both hyper- and hypophosphorylated forms of RB remained at steady-state levels (Figure 3A, lanes 5–7), although the hypophosphorylated form seemed dominant at PD 53 (Figure 3A, lane 6), perhaps due to the higher cell density at collection of cell lysate. The protein level of RB was down-regulated in E7-overexpressing UCBE6E7-20 cells (Figure 3A, lane 8), probably as a result of enhanced proteolysis by E7.

Increase in Telomerase Activity and Maintenance of Telomere Length in Cells Transduced with the hTERT

Telomerase activity is revealed by the characteristic six base pair ladder of bands detected by TRAP assay (Figure 4A). No telomerase activity was detected in UCBMSCs at any PDs tested, UCBE6E7-20 cells, UCBMSCs infected with the vector-alone or CHAPS buffer, or mock infected. By contrast, the cells transduced with the hTERT exhibited significant levels of telomerase activity, comparable to HeLa cells as a positive control and to TSR8, which is a synthetic template of eight telomeric repeats used as a polymerase chain reaction (PCR)-positive control.

Average telomere length was longer in the UCBTERT-21 cells than in UCBMSCs. Telomere length in UCBMSCs decreased with the number of PDs, whereas it remained the same in UCBTERT-21 cells, regardless of the number of PDs. The telomere length of UCBE6E7-20 cells was shorter than that of the parental UCBMSCs at senescence.

Normal Diploid Karyotypes with XY Sex Chromosomes in UCBMSCs and UCBTERT-21 Cells

Karyotypic analyses of UCBMSCs were performed at PD 5 (2 passages) and of UCBTERT-21 cells at PD 32 (14 passages). UCBMSCs and UCBTERT-21 cells were found to be diploid and not to exhibit any significant chromosomal abnormalities (Figure 5, A and B). The chromosome number of both UCBMSCs at PD 5 and UCBTERT-21 cells at PD 35 was 46, except for one UCBTERT-21 cell, which contained 47 chromosomes (Figure 5C). No UCBTERT-21 cells containing abnormal numbers of chromosome were found on further analysis. The sex chromosomes were found to be XY, indicating that the cells were of fetal origin.

Osteogenic and Adipogenic Differentiation Potentials of UCBMSCs and UCBTERT-21 Cells

The multipotency of UCBMSCs and UCBTERT-21 cells was assessed by conventional protocols. The osteogenic differentiation potential of UCBMSCs and UCBTERT-21 cells was assessed based on their morphology and von Kossa staining after 3 wk of induction (Figure 6). Multiple small Oil-Red-O–positive fat droplets had accumulated in UCBMSCs and UCBTERT-21 cells after 3 and 2 wk, respectively, of adipogenic induction. Adipocyte differentiation was estimated by counting 2000 cells per dish. The results of triplicate experiments showed that 5.0 and 5.4% of the UCBMSC and UCBTERT-21 cells became positive for fat droplets with Oil-Red stain as a result of adipogenic induction and >90% of the cells were positive on ALP staining after osteogenic induction. We also induced these cells to differentiate into multiple lineages by the methods for neural (Kohyama *et al.*, 2001), cardiomyogenic (Makino *et al.*, 1999; Takeda *et al.*, 2004), and chondrogenic (Imabayashi *et al.*, 2003) lineages; however, the UCBMSC and UCBTERT-21 cells were not induced to differentiate into these lineages in vitro.

DISCUSSION

This study was undertaken to obtain human UCB-derived fetal cells that retain critical cell functions, the same as bone marrow-derived mesenchymal stem cells, mammary gland

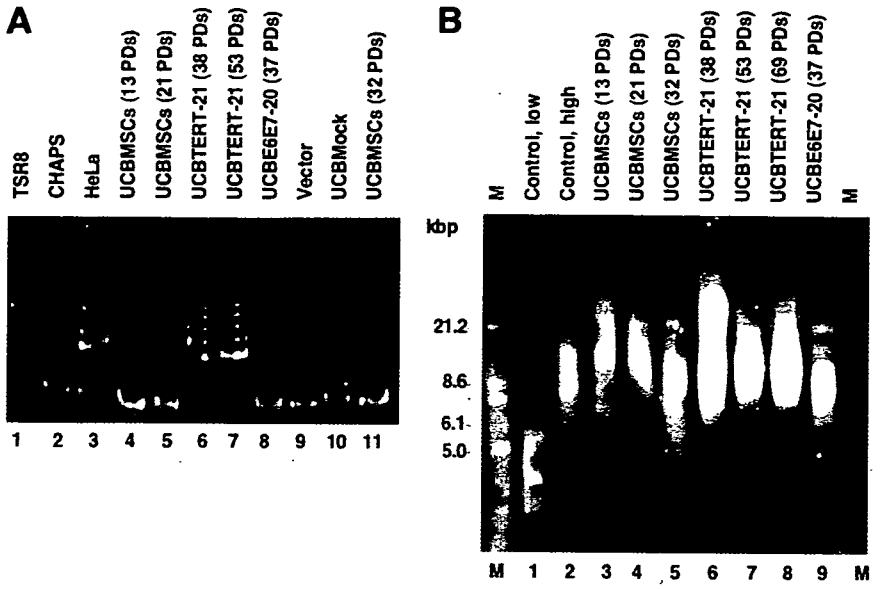

Figure 4. Telomerase activity and telomere length of UCBMSCs, UCBE6E7-20 cells, and UCBTERT-21 cells. (A) Analysis of telomerase activity by the PCR assay in UCBMSCs, UCBE6E7-20 cells, and UCBTERT-21 cells. Telomerase activity is revealed by the characteristic six-base pair ladder of bands. No telomerase activity was detected in the UCBMSCs at PD 13, 21, or 32 (lanes 4, 5, and 11, respectively), the UCBE6E7-20 cells at PD 37 (lane 8), the UCBMSCs infected with the vector alone (lane 9), the CHAPS buffer alone (lane 2) or Mock infected cells (lane 10). By contrast, the UCBTERT-21 cells at PD 38 and 53 exhibited significant telomerase activity (lanes 6 and 7, respectively) that was comparable with that of the HeLa cells (lane 3) and TSR8 (lane 1) as positive controls. (B) Telomere length of UCBMSCs, UCBE6E7-20 cells, and UCBTERT-21 cells. Telomere length was longer in the UCBTERT-21 cells than in the parental UCBMSCs. The telomere length of UCBMSCs at PD 13, 21, and 32 decreased as the number of PDs increased (lanes 3–5). The telomere length of UCBTERT-21 cells was maintained, irrespective of the number of PDs (lanes 6–8). The telomere length of UCBE6E7-20 cells at PD 37 (lane 9) was shorter than that of the parental UCBMSCs at PD 32 (lane 5). Lanes 1 and 2 are control DNAs of short length and long length, respectively.

epithelial cells, skin keratinocytes, and pigmented epithelial cells. It may be possible to use human UCB- and bone marrow-derived stem cells in the future clinically to supply defective enzymes to patients with genetic metabolic diseases, such as neuro-Gaucher disease, Fabry disease, and mucopolysaccharidosis, whose prognosis is poor, and is sometimes lethal. To achieve this, we attempted to prolong the life span of UCB-derived cells or to endow them with immortality without transformation, defining "immortality" simply as indefinite cell division.

Is Successful Prolongation of UCBMSCs Life Span without Inhibition of the p16^{INK4a}/RB Pathway Attributable to a Lack of Ex Vivo Culture Stress?

In contrast to our previous study by using bone marrow-derived cells (Takeda *et al.*, 2004), surprisingly, the successful prolongation of the life span of the UCB-derived fetal cells obtained in this study did not require inhibition of the p16^{INK4a}/RB pathway or premature senescence-associated pathway. Immortalization of some human cell types requires inhibition of the p16^{INK4a}/RB pathway in addition to activation of telomerase (Kiyono *et al.*, 1998; Ishikawa, 2003). Human mammary epithelial cells, endometrial glandular cells, skin keratinocytes, and marrow-derived cells require inhibition of the p16^{INK4a}/RB pathway for immortalization, but foreskin fibroblasts do not. Activation of telomerase alone is sufficient for immortalization of human foreskin fibroblasts. HPV16 E6 and E7 have been used to inhibit p53 and RB, respectively, to prolong the life span of marrow-derived MSCs (Okamoto *et al.*, 2002; Takeda *et al.*, 2004), endometrial gland cells (Kyo *et al.*, 2003), mammary epithelial cells, and keratinocytes (Kiyono *et al.*, 1998). Bmi-1 also has been used to inhibit p16^{INK4a} transcription to prolong the life span of marrow-derived MSCs. One function of this p16INK4a protein is to maintain pRB in a hypophosphorylated active form, which inhibits cell cycle progression.

Our present findings that UCB-derived cells can be immortalized without inhibition of the p16^{INK4a}/RB pathway is consistent with the results in regard to foreskin fibroblasts. This successful immortalization of UCB-cells by hTERT alone can be explained by lack of ex vivo culture stress under the culture condition used in this study. Alternatively, only cells insensitive to ex vivo culture stress or lacking p16^{INK4a} induction may be expanded by hTERT alone. Primary UCB-derived cell culture succeeded in 94% of the attempts (15 of 16 trials), and the cells were passaged only two or three times before reaching premature senescence (13 of 15 primary UCB-derived cell cultures); however, only two cell strains (UCBMSCs) were established from them (2 of 15 primary UCB-derived cell cultures; see *Materials and Methods*. "Isolation and Cell Culture of UCBMSCs"). Based on the results of this study by using one of the two cell strains, the establishment of these strains (UCBMSCs) can be explained by 1) lack of p16^{INK4a} in primary cultured UCB-derived cells or 2) selection of cells that do not express p16^{INK4a} from a heterogeneous population. We cannot exclude either possibilities, and we did observe two different types of cells, i.e., rapidly growing cells and quiescent cells in the primary culture of cord blood cells. If the alternative explanation is true, these quiescent cells, in which p16^{INK4a} may be expressed at a high level, can be efficiently expanded by introduction of E7, the inhibitor of RB, or Bmi-1, the down-regulator of p16^{INK4a}. We also performed additional experiments by using newly obtained specimens from umbilical cord to determine whether infection of the primary or first passage cells generates long-term strains routinely and efficiently. We generated other cells, UCB408 cells, and found that generation of long-term strains was reproducible (Supplementary Figure A). The UCBE6E7-31 and UCBE7-32 cells proliferated for >30 PDs and exhibited persistent growth. The UCBTERT-30 cells exhibited a prolonged cell life span in culture and reached PD 19, but they failed to be immortalized. The success of immortalization of UCBMSCs may still be low, probably due to expression of p16^{INK4a} premature senescence-associated proteins in the early passage of the UCB408 cells. Because the 5′ CpG island of the p16^{INK4a} promoter based on published genome sequences (GenBank accession no. AF022809, U12818, and AC000048) has been found to be methylation-free by the bisulfite method (Supplementary Figures B and C), the lack of

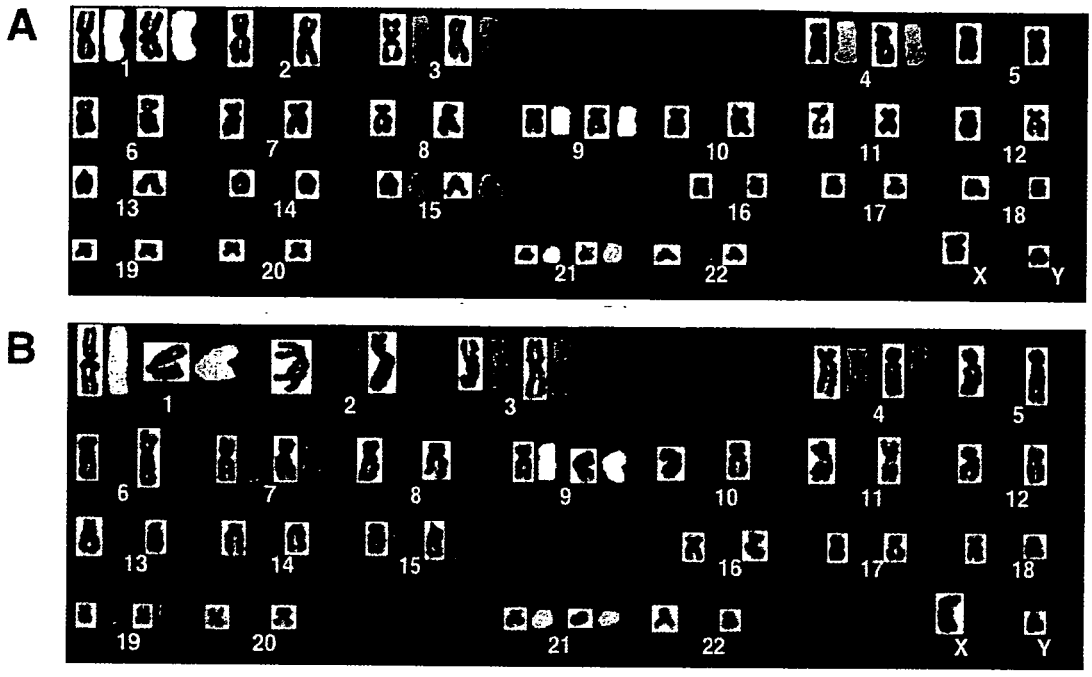

C

Chromosome number		44	45	46	47	48
Number of cells	UCBMSCs, PD5	0	0	50	0	0
	UCBTERT-21, PD35	0	0	49	1	0

Figure 5. Karyotypic analysis of UCBMSCs and UCBTERT-21 cells. Comprehensive karyotyping (left side, reverse DAP, right side, SKY), UCBMSCs at PD 5 (A) and UCBTERT-21 cells at PD 35 (B). Normal diploidy is seen in the UCBMSCs and UCBTERT-21 cells. Both cells were analyzed for chromosome number (C). None of the 50 UCBMSCs tested showed any abnormal numbers of chromosomes. Of the 50 UCBTERT-21 cells tested, 49 exhibited normal diploidy and one cell contained 47 chromosomes. No UCBTERT-21 cells with an abnormal chromosome number were found on further analysis.

$p16^{INK4a}$ expression in rapidly growing cells is not due to methylation of the $p16^{INK4a}$ promoter, unlike human mammary epithelial cells (Umezawa *et al.*, 1997; Foster *et al.*, 1998; Wong *et al.*, 1999).

UCB-derived Cells Are of Mesenchymal Origin

The differentiation capacity of UCB-derived cells was unaffected during establishment of a plate-adhering population of cells from UCB. The cells established from UCB can be extensively and clonally expanded in vitro while retaining their potential to differentiate into osteoblasts that produce mineralized matrices and adipocytes that accumulate lipid vacuoles under in vitro conditions. This differentiation potential of the UCB-derived cells is the same as that reported for bone marrow MSCs (Goodwin *et al.*, 2001; Lee *et al.*, 2004).

The surface markers of the UCB-derived cells examined in this study are exactly the same as those of previously reported UCB-derived cells (Lee *et al.*, 2004). Most of the surface markers are the same as those detected in their bone marrow counterparts (Takeda *et al.*, 2004), with both UCB- and bone marrow-derived cells being positive for CD29, CD44, CD55, and CD59, and negative for CD34 and CD117. The CD90 and CD133 markers, on the other hand, can be used to distinguish UCB-derived cells from bone marrow-derived cells, because they are both expressed in multipotent marrow-derived cells (Takeda *et al.*, 2004) and not in UCB-derived cells (Figure 2) (Lee *et al.*, 2004).

This technique allows the applications of UCB to be further extended and permits it to be used as an alternative to bone marrow as a source of hMSCs; however, this study puts the controversy to rest and substantiates that UCB does contain hMSCs. We believe that the "UCBMSCs" are mesenchymal stem cells derived from UCB, as designated. However, it is difficult to exclude the possibility that the UCBMSCs were derived from mesenchymal cells embedded in the Wharton's jelly of the umbilical cord during insertion of the needle into the vessels through the umbilical cord.

Can primary UCB-derived cell "culture" contribute to cell-based therapy or regenerative medicine? The problems involved in cell-based therapy with human UCB-derived cells are the finite cell life span of the cells and the difficulty of obtaining a large enough number of cells. The technique that allows human cells to escape senescence used in this study may be used to obtain a large number of cells and to overcome these problems of a short life span.

ACKNOWLEDGMENTS

We thank members of Virology Division, National Cancer Center Research Institute (Tokyo, Japan) for helpful discussion and continuous encouragement

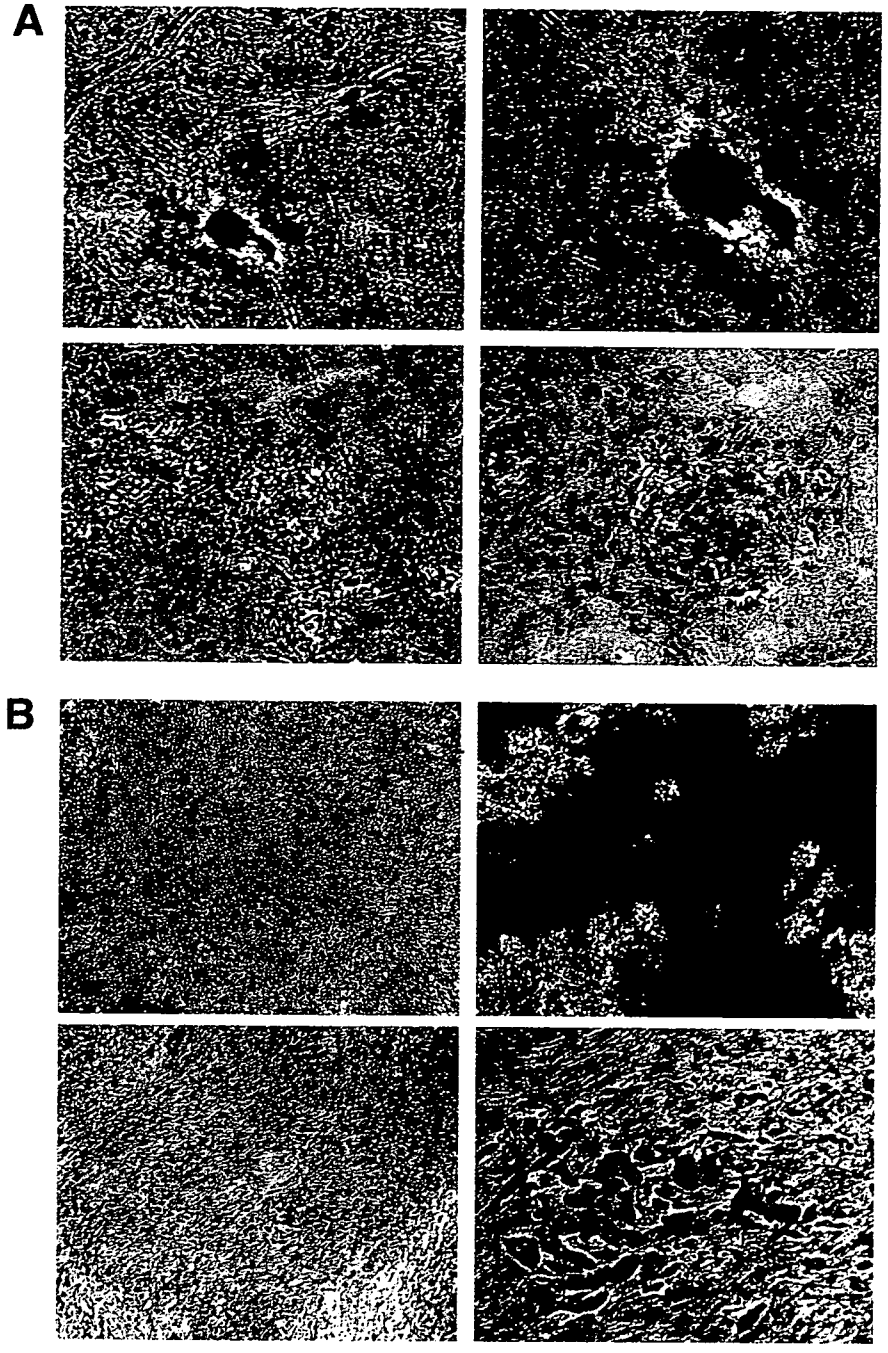

Figure 6. Osteogenic and adipogenic differentiation of UCBMSCs and UCBTERT-21 cells. UCBMSCs (A) and UCBTERT-21 cells (B) were examined by von Kossa staining after 3 wk of osteogenic induction (A and B, top columns) and by Oil-Red-O staining after 2 wk of adipogenic induction (A and B, bottom columns). Both cells contained small lipid vacuoles in their cytoplasm. Original magnifications: (A) left column, 10×; right column, 20×; (B) left column, 5×; right column, 20×.

of this research. This study was supported by a grant from the Ministry of Education, Culture, Sports, Science, and Technology (MEXT) of Japan and the Health and Labor Sciences Research grants (to A. U. and T. K.); the Pharmaceuticals and Medical Devices Agency (to A. U.); an Award for Research Resident Fellowship from the Japan Health Sciences Foundation (to M. T.); and the Japan Association for the Advancement of Medical Equipment (to T. U.).

REFERENCES

Blackburn, E. H. (2000a). Telomere states and cell fates. Nature *408*, 53–56.

Blackburn, E. H. (2000b). Telomeres and telomerase. Keio J. Med. *49*, 59–65.

Blackburn, E. H. (2001). Switching and signaling at the telomere. Cell *106*, 661–673.

Burk, R. D., *et al.* (2003). Distribution of human papillomavirus types 16 and 18 variants in squamous cell carcinomas and adenocarcinomas of the cervix. Cancer Res. *63*, 7215–7220.

Campisi, J. (1997). The biology of replicative senescence. Eur. J. Cancer *33*, 703–709.

Caplan, A. I. (1991). Mesenchymal stem cells. J. Orthop. Res. *9*, 641–650.

Caplan, A. I., and Bruder, S. P. (2001). Mesenchymal stem cells: building blocks for molecular medicine in the 21st century. Trends Mol. Med. *7*, 259–264.

D'Ippolito, G., Schiller, P. C., Ricordi, C., Roos, B. A., and Howard, G. A. (1999). Age-related osteogenic potential of mesenchymal stromal stem cells from human vertebral bone marrow. J. Bone Miner. Res. *14*, 1115–1122.

Dimri, G. P., *et al.* (1995). A. biomarker that identifies senescent human cells in culture and in aging skin in vivo. Proc. Natl. Acad. Sci. USA *92*, 9363–9367.

Foster, S. A., Wong, D. J., Barrett, M. T., and Galloway, D. A. (1998). Inactivation of p16 in human mammary epithelial cells by CpG island methylation. Mol. Cell. Biol. *18*, 1793–1801.

Gewin, L., Myers, H., Kiyono, T., and Galloway, D. A. (2004). Identification of a novel telomerase repressor that interacts with the human papillomavirus type-16 E6/E6-AP complex. Genes Dev. *18*, 2269–2282.

Goodwin, H. S., Bicknese, A. R., Chien, S. N., Bogucki, B. D., Quinn, C. O., and Wall, D. A. (2001). Multilineage differentiation activity by cells isolated from umbilical cord blood: expression of bone, fat, and neural markers. Biol. Blood Marrow Transplant *7*, 581–588.

Hayflick, L. (1976). The cell biology of human aging. N. Engl. J. Med. *295*, 1302–1308.

Imabayashi, H., Mori, T., Gojo, S., Kiyono, T., Sugiyama, T., Irie, R., Isogai, T., Hata, J., Toyama, Y., and Umezawa, A. (2003). Redifferentiation of dedifferentiated chondrocytes and chondrogenesis of human bone marrow stromal cells via chondrosphere formation with expression profiling by large-scale cDNA analysis. Exp. Cell Res. *288*, 35–50.

Ishikawa, F. (2003). Cellular senescence, an unpopular yet trustworthy tumor suppressor mechanism. Cancer Sci. *94*, 944–947.

Jaiswal, N., Haynesworth, S. E., Caplan, A. I., and Bruder, S. P. (1997). Osteogenic differentiation of purified, culture-expanded human mesenchymal stem cells in vitro. J. Cell. Biochem. *64*, 295–312.

Jiang, Y., *et al.* (2002). Pluripotency of mesenchymal stem cells derived from adult marrow. Nature *418*, 41–49.

Kiyono, T., Foster, S. A., Koop, J. I., McDougall, J. K., Galloway, D. A., and Klingelhutz, A. J. (1998). Both Rb/p16^{INK4a} inactivation and telomerase activity are required to immortalize human epithelial cells. Nature *396*, 84–88.

Kohyama, J., Abe, H., Shimazaki, T., Koizumi, A., Nakashima, K., Gojo, S., Taga, T., Okano, H., Hata, J., and Umezawa, A. (2001). Brain from bone: efficient "meta-differentiation" of marrow stroma-derived mature osteoblasts to neurons with Noggin or a demethylating agent. Differentiation *68*, 235–244.

Kyo, S., Nakamura, M., Kiyono, T., Maida, Y., Kanaya, T., Tanaka, M., Yatabe, N., and Inoue, M. (2003). Successful immortalization of endometrial glandular cells with normal structural and functional characteristics. Am. J. Pathol. *163*, 2259–2269.

Lee, O. K., Kuo, T. K., Chen, W. M., Lee, K. D., Hsieh, S. L., and Chen, T. H. (2004). Isolation of multipotent mesenchymal stem cells from umbilical cord blood. Blood *103*, 1669–1675.

Makino, S., *et al.* (1999). Cardiomyocytes can be generated from marrow stromal cells in vitro. J. Clin. Investig. *103*, 697–705.

Mayani, H., and Lansdorp, P. M. (1998). Biology of human umbilical cord blood-derived hematopoietic stem/progenitor cells. Stem Cells *16*, 153–165.

Okamoto, T., Aoyama, T., Nakayama, T., Nakamata, T., Hosaka, T., Nishijo, K., Nakamura, T., Kiyono, T., and Toguchida, J. (2002). Clonal heterogeneity in differentiation potential of immortalized human mesenchymal stem cells. Biochem. Biophys. Res. Commun. *295*, 354–361.

Owen, M. (1988). Marrow stromal stem cells. J. Cell Sci. Suppl. *10*, 63–76.

Pittenger, M. F., Mackay, A. M., Beck, S. C., Jaiswal, R. K., Douglas, R., Mosca, J. D., Moorman, M. A., Simonetti, D. W., Craig, S., and Marshak, D. R. (1999). Multilineage potential of adult human mesenchymal stem cells. Science *284*, 143–147.

Prockop, D. J. (1997). Marrow stromal cells as stem cells for nonhematopoietic tissues. Science *276*, 71–74.

Prockop, D. J., Sekiya, I., and Colter, D. C. (2001). Isolation and characterization of rapidly self-renewing stem cells from cultures of human marrow stromal cells. Cytotherapy *3*, 393–396.

Sasaki, M. S. (1975). A comparison of chromosomal radiosensitivities of somatic cells of mouse and man. Mutat. Res. *29*, 433–448.

Sekiguchi, T., and Hunter, T. (1998). Induction of growth arrest and cell death by overexpression of the cyclin-Cdk inhibitor p21 in hamster BHK21 cells. Oncogene *16*, 369–380.

Sekiguchi, T., Nishimoto, T., and Hunter, T. (1999). Overexpression of D-type cyclins, E2F-1, SV40 large T antigen and HPV16 E7 rescue cell cycle arrest of tsBN462 cells caused by the CCG1/TAF(II)250 mutation. Oncogene *18*, 1797–1806.

Sekiya, I., Larson, B. L., Vuoristo, J. T., Cui, J. G., and Prockop, D. J. (2004). Adipogenic differentiation of human adult stem cells from bone marrow stroma (MSCs). J. Bone Miner. Res. *19*, 256–264.

Takeda, Y., *et al.* (2004). Can the life span of human marrow stromal cells be prolonged by bmi-1, E6, E7, and/or telomerase without affecting cardiomyogenic differentiation? J. Gene Med. *6*, 833–845.

Tsuchiya, K., Mori, T., Chen, G., Ushida, T., Tateishi, T., Matsuno, T., Sakamoto, M., and Umezawa, A. (2004). Custom-shaping system for bone regeneration by seeding marrow stromal cells onto a web-like biodegradable hybrid sheet. Cell Tissue Res. *316*, 141–153.

Umezawa, A., Maruyama, T., Segawa, K., Shadduck, R. K., Waheed, A., and Hata, J. (1992). Multipotent marrow stromal cell line is able to induce hematopoiesis in vivo. J. Cell. Physiol. *151*, 197–205.

Umezawa, A., Yamamoto, H., Rhodes, K., Klemsz, M. J., Maki, R. A., and Oshima, R. G. (1997). Methylation of an ETS site in the intron enhancer of the keratin 18 gene participates in tissue-specific repression. Mol. Cell. Biol. *17*, 4885–4894.

Vaziri, H., Dragowska, W., Allsopp, R. C., Thomas, T. E., Harley, C. B., and Lansdorp, P. M. (1994). Evidence for a mitotic clock in human hematopoietic stem cells: loss of telomeric DNA with age. Proc. Natl. Acad. Sci. USA *91*, 9857–9860.

Wong, D. J., Foster, S. A., Galloway, D. A., and Reid, B. J. (1999). Progressive region-specific de novo methylation of the p16 CpG island in primary human mammary epithelial cell strains during escape from M(0) growth arrest. Mol. Cell. Biol. *19*, 5642–5651.

MOLECULAR AND CELLULAR BIOLOGY, Jan. 2005, p. 136–146 Vol. 25, No. 1
0270-7306/05/$08.00+0 doi:10.1128/MCB.25.1.136–146.2005

Cyclic AMP Potentiates Vascular Endothelial Cadherin-Mediated Cell-Cell Contact To Enhance Endothelial Barrier Function through an Epac-Rap1 Signaling Pathway

Shigetomo Fukuhara,[1] Atsuko Sakurai,[1] Hideto Sano,[2] Akiko Yamagishi,[1] Satoshi Somekawa,[1,3] Nobuyuki Takakura,[2] Yoshihiko Saito,[3] Kenji Kangawa,[4] and Naoki Mochizuki[1]*

Department of Structural Analysis[1] and Department of Biochemistry,[4] National Cardiovascular Center Research Institute, Osaka, Department of Stem Cell Biology, Cancer Research Institute, Kanazawa University, Kanazawa,[2] and First Department of Internal Medicine, Nara Medical University, Nara,[3] Japan

Received 2 August 2004/Returned for modification 2 September 2004/Accepted 28 September 2004

Cyclic AMP (cAMP) is a well-known intracellular signaling molecule improving barrier function in vascular endothelial cells. Here, we delineate a novel cAMP-triggered signal that regulates the barrier function. We found that cAMP-elevating reagents, prostacyclin and forskolin, decreased cell permeability and enhanced vascular endothelial (VE) cadherin-dependent cell adhesion. Although the decreased permeability and the increased VE-cadherin-mediated adhesion by prostacyclin and forskolin were insensitive to a specific inhibitor for cAMP-dependent protein kinase, these effects were mimicked by 8-(4-chlorophenylthio)-2′-*O*-methyladenosine-3′, 5′-cyclic monophosphate, a specific activator for Epac, which is a novel cAMP-dependent guanine nucleotide exchange factor for Rap1. Thus, we investigated the effect of Rap1 on permeability and the VE-cadherin-mediated cell adhesion by expressing either constitutive active Rap1 or Rap1GAPII. Activation of Rap1 resulted in a decrease in permeability and enhancement of VE-cadherin-dependent cell adhesion, whereas inactivation of Rap1 had the counter effect. Furthermore, prostacyclin and forskolin induced cortical actin rearrangement in a Rap1-dependent manner. In conclusion, cAMP-Epac-Rap1 signaling promotes decreased cell permeability by enhancing VE-cadherin-mediated adhesion lined by the rearranged cortical actin.

Endothelial cells lining blood vessels regulate endothelial barrier function, which restricts the passage of plasma proteins and circulating cells across the endothelial cells. Endothelial barrier dysfunction results in an increase in vascular permeability, thereby causing edema or inflammatory or metastatic cell infiltration. Inflammatory mediators such as thrombin and histamine induce intercellular gap formation, leading to an increase in endothelial permeability (1, 4). In contrast, angiopoietin 1 and sphingosine-1-phosphate (S1P) stabilize endothelial barrier integrity (17, 18). In addition, cyclic AMP (cAMP), a second messenger downstream of Gs-coupled receptor, improves endothelial cell barrier function (32, 39, 43). Consistently, cAMP-elevating G protein-coupled receptor (GPCR) agonists, adrenomedullin (AM), prostacyclin (PGI2), prostaglandin E2 (PGE2), and β-adrenergic agonists reduce endothelial hyperpermeability induced by inflammatory stimuli (15, 19, 25).

The endothelial cell barrier is structurally organized by adherens junctions (AJ) and tight junctions. Vascular endothelial (VE) cells express both VE-cadherin (also known as cadherin-5 and CD144) and neural (N)-cadherin (9, 33). VE-cadherin constitutes AJ, whereas N-cadherin formed the cell-cell contacts between endothelial cells and endothelial cell-supporting pericytes. VE-cadherin mediates calcium-dependent, homophilic intercellular adhesion. Its short cytoplasmic tail binds to three armadillo family proteins, β-, γ-, and p120-catenins. β- and γ-catenins associated with α-catenin link the VE-cadherin complex to the actin cytoskeleton and, therefore, strengthen the AJ adhesiveness (9).

Endothelial AJ are dynamic structures, and their adhesive property is finely regulated by several different mechanisms. Tyrosine phosphorylation of VE-cadherin, β-catenin, and p120-catenin correlates with weakened endothelial cell-cell adhesion. VE growth factors and inflammatory mediators such as histamine and thrombin induce tyrosine phosphorylation of AJ components, resulting in the weakened cell-cell contacts and increased endothelial cell permeability (1, 14, 40). In clear contrast, angiopoietin 1, which stabilizes cell-cell contacts, induces dephosphorylation of endothelial cell adhesion molecules, VE-cadherin, and platelet endothelial cell adhesion molecule 1 (17). It has been also reported that S1P induces AJ formation and enhances barrier function through a Rac-dependent cortical actin rearrangement (18). cAMP-dependent protein kinase A (PKA) is suggested to be crucial for cAMP-triggered stabilization of cell-cell contacts and for barrier integrity of endothelial cells (43). However, it has not been clear whether PKA-independent signaling is involved in the regulation of endothelial barrier function.

Rap1, belonging to Ras family GTPase, is involved in the formation and stabilization of AJ in *Drosophila melanogaster* (23). Rap1 becomes the GTP-bound active form by guanine

* Corresponding author. Mailing address: Department of Structural Analysis, National Cardiovascular Center Research Institute, 5-7-1 Fujishirodai, Suita, Osaka 565-8565, Japan. Phone: 81-6-6833-5012, ext. 2508. Fax: 81-6-6835-5461. E-mail: nmochizu@ri.ncvc.go.jp.

nucleotide exchange factor (GEF) and the GDP-bound inactive form by GTPase-activating proteins (GAP), respectively. GEFs for Rap1 include C3G, CalDAG-GEFs, Epacs, and DOCK4 (reviewed in reference 6). DOCK4, which is disrupted in various types of human cancers, regulates the formation of AJ (41). Very recent reports also revealed that Rap1 activity is required for the formation of E-cadherin-based cell-cell contacts (20, 36). These findings prompted us to investigate how Rap1 is activated to stabilize cell-cell contacts and to examine the physiological consequence of stabilized cell-cell contacts by Rap1.

In the present study, we investigated the mechanism by which cAMP-elevating GPCR agonists potentiate endothelial barrier function and restrict cell permeability. We found that increased cAMP triggers Epac-Rap1 signaling to reduce permeability independently of PKA by augmentation of VE-cadherin-mediated cell-cell adhesion.

MATERIALS AND METHODS

Reagents and antibodies. Human recombinant AM was kindly provided by Shionogi & Co. Ltd (31). Materials were purchased as follows: isoproterenol (Iso), PGE2, PGI2, thrombin, forskolin (FSK), and 3-isobutyl-1-methylxanthine (IBMX) from Wako Pure Chemical Industries; dibutyryl-cAMP (dbcAMP) from Sigma-Aldrich; H89 from Seikagaku Corporation; 8-(4-chlorophenylthio)-2′-*O*-methyladenosine-3′,5′-cyclic monophosphate (8-CPT-2′-O-Me-cAMP) from Tocris; fluorescein isothiocyanate (FITC)-labeled dextran (molecular weight, 42,000) and purified human immunoglobulin G (IgG) Fc protein from ICN Biologicals; vascular endothelial growth factor (VEGF) from R & D Systems. Anti-Rap1GAPII antibody was developed by immunization of glutathione *S*-transferase (GST)-tagged Rap1GAPII (amino acids 411 to 694 of Rap1GAPII). Other antibodies used here were purchased as follows: anti-VE-cadherin from Chemicon International and Transduction Laboratories; anti-β-catenin from Transduction Laboratories; anti-CREB and anti-phospho-CREB (Ser133) from Cell Signaling Technology; anti-Rap1 from Santa Cruz Biotechnology; anti-cortactin from Upstate Biotechnology, Inc.; rhodamine-phalloidin and Alexa 488-labeled goat anti-mouse IgG from Molecular Probes; horseradish peroxidase-coupled goat anti-mouse and goat anti-rabbit IgG from Amersham Biosciences.

Cell culture and transfection. Human umbilical vein endothelial cells (HUVECs) and human arterial endothelial cells (HAECs) were purchased from Kurabo (Kurashiki, Japan). The cells were maintained in HuMedia-EG2 with a growth additive set as described previously (12) and used for experiments before passages 7 and 10, respectively. HEK293, 293T, and HeLa cells were maintained in Dulbecco's modified Eagle's medium (DMEM; Nissui, Tokyo, Japan) supplemented with 10% fetal bovine serum and antibiotics (100 μg of streptomycin/ml and 100 U of penicillin/ml). HUVECs and 293T cells were transfected by using Lipofectamine Plus reagent (Invitrogen) and by the calcium-phosphate precipitation technique, respectively.

Plasmids and adenovirus. pcDNA-VE-cad-Ect-Fc-His is a modified vector of pcDNA3.1-Fc-PECAM-1 (a kind gift from W. A. Muller, Cornell University) for producing the secreted form of the extracellular domain of VE-cadherin fused with Fc followed by a six-His tag. A DNA fragment encoding human Epac lacking the cAMP binding domain (amino acids 324 to 881) was amplified by PCR with pMT2SM-HA-Epac (a kind gift from J. L. Bos, Utrecht University, Utrecht, The Netherlands) as a template and ligated into the pCXN2 vector (12). pCXN2-FLAG-Rap1V12-IRES-EGFP expressed both FLAG-tagged Rap1V12 and internal ribosomal entry site (IRES)-driven enhanced green fluorescent protein (EGFP), and pCXN2-Rap1GAPII-IRES-EGFP expressed both FLAG-tagged Rap1GAPII and IRES-driven EGFP. pGL3 control vector was purchased from Promega Corp. Recombinant adenoviruses encoding Rap1GAPII (Ad-RapGAP) and LacZ (Ad-LacZ) were obtained from S. Hattori (The Institute of Medical Science, University of Tokyo) and M. Matsuda (Research Institute for Microbial Disease, Osaka University, Osaka, Japan), respectively. Adenoviruses expressing FLAG-tagged Rap1V12 and IRES-driven EGFP (Ad-Flag-Rap1V12-IRES-EGFP) were produced by using the Adeno-X system according to the manufacturer's protocol (Clontech). Endothelial cells were infected with adenoviruses at the appropriate multiplicities of infection (MOI) as described in the figure legends.

Permeability assay. Permeability across the endothelial cell monolayer was measured by using type I collagen-coated transwell units (6.5-mm diameter, 3.0-μm-pore-size polycarbonate filter; Corning Costar Corporation). HUVECs plated at 10^5 cells in each well were cultured for 3 to 4 days before experiments. After serum starvation in medium 199 containing 1% bovine serum albumin (BSA) for 1 h, the cells were treated with the agonists or drugs, as indicated in the figure legends, for 30 min. Permeability was measured by adding 1 mg of FITC-labeled dextran (molecular weight, 42,000)/ml together with or without 2 U of thrombin/ml to the upper chamber. After incubation for 30 min, 50 μl of sample from the lower compartment was diluted with 300 μl of phosphate-buffered saline (PBS) and measured for fluorescence at 520 nm when excited at 492 nm with a spectrophotometer F-4500 (Hitachi). HUVECs infected with adenovirus for 24 h after becoming confluent and kept for another 24 h in replaced medium were subjected to a cell permeability assay.

Immunocytochemistry. Monolayer-cultured HUVECs grown on a 35-mm-diameter glass base dish (Asahi Techno Glass) were starved in medium 199 containing 0.5% BSA for 3 h and subsequently incubated with the stimulants indicated in the figure legends for 30 min. After stimulation, the cells were fixed in PBS containing 2% formaldehyde for 30 min at 4°C, washed with PBS, and permeabilized with 0.05% Triton X-100 for 30 min at 4°C. Cells were blocked with PBS containing 4% BSA for 1 h at room temperature (RT) and stained with rhodamine-phalloidin for 20 min, anti-VE-cadherin for 60 min, and anticortactin for 60 min at RT. Protein reacting with antibody was visualized with Alexa 488-labeled goat anti-mouse IgG. Images were recorded with a confocal microscope (BX50WI, Fluoview; Olympus) with a water immersion objective lens (LUMPlanF1 100X1.00W).

VE-cadherin translocation assay and Western blot analysis. HUVECs plated in six-well plates were serum starved in medium 199 containing 1% BSA overnight. The cells were stimulated with PGI2 and FSK for the indicated time and fractionated with cytoskeleton-stabilizing buffer (10 mM HEPES [pH 7.4], 250 mM sucrose, 150 mM KCl, 1 mM EGTA, 3 mM $MgCl_2$, 1× protease inhibitor cocktail [Roche Diagnostics], 1 mM Na_3VO_4, 0.5% Triton X-100) by centrifugation at 15,000 × *g* for 15 min. The Triton X-100-insoluble fraction was subjected to sodium dodecyl sulfate-polyacrylamide gel electrophoresis (SDS-PAGE) followed by transfer to Immobilon-P (Amersham Biosciences) and immunoblotting with the indicated antibodies. Immunocomplexes were visualized by enhanced chemiluminescence detection (Amersham Biosciences) with species-matched peroxidase-conjugated secondary antibodies.

Purification of recombinant VE-cadherin ectodomain-Fc chimeric protein. 293T cells transfected with pcDNA-VE-cad-Ect-Fc-His were cultured in DMEM supplemented with 10% fetal calf serum for 24 h and subsequently kept in replaced medium (DMEM-F21 containing 1% fetal calf serum) for 7 days. VE-cadherin-Fc (VEC-Fc) protein secreted into the medium was collected every 2 days and centrifuged to remove floating cells and debris. VEC-Fc was collected on ProBond resin (Invitrogen) by gentle agitation overnight at 4°C. VEC-Fc protein bound to the beads was eluted with 500 mM imidazole, concentrated with Amicon Centriplus 30 (Millipore), and buffer exchanged into PBS containing 2 mM $CaCl_2$ and 2 mM $MgCl_2$ (PBS-Ca/Mg) by dialysis.

Cell adhesion assay. Twenty-four-well tissue culture plates were coated with 10 μg of VEC-Fc or Fc protein/ml in PBS-Ca/Mg at 4°C overnight. After washing with PBS-Ca/Mg, the plates were blocked with 1% heat-inactivated BSA in PBS (heat inactivated at 85°C for 12 min) for 1 h at RT. To examine cell adhesion to the VEC-Fc- or Fc-coated dish, cells were suspended in 0.5% BSA-containing medium 199 and incubated for 30 min at 37°C. Cells (1.5×10^5) were plated on each VEC-Fc- or Fc-coated well in the presence or absence of agonists, drugs, and 5 mM EGTA and adhered to the dish at 37°C for the indicated time. To analyze cell adhesion to a collagen-covered surface, cells were plated onto a collagen-coated six-well plate (Iwaki) and adhered to the dish in the presence or absence of 5 mM EGTA. After washing with PBS-Ca/Mg four times to remove nonadherent cells, adherent cells and input cells were quantified by measuring endogenous alkaline phosphatase activity as described elsewhere (35). Briefly, the cells were lysed in a buffer containing 100 mM Tris-citrate (pH 6.5) and 0.25% Triton X-100, and alkaline phosphate activity in the lysate was measured by using the AttoPhos AP fluorescent substrate system (Promega Corp.). To examine the effects of Rap1V12, EpacΔcAMP, and Rap1GAPII, HUVECs were transfected with plasmids encoding either Rap1V12, EpacΔcAMP, or Rap1GAPII together with the luciferase reporter construct (pGL3 control vector). The adhesion of cells expressing Rap1V12, EpacΔcAMP, or Rap1GAPII to the VEC-Fc-coated dish was normalized by measuring the luciferase activity of the cells and input cells (16).

Detection of GTP-bound form of Rap1. Rap1 activity was assessed by a modified Bos's method as described previously (34). Briefly, HUVECs starved in medium 199 containing 1% BSA overnight were stimulated with the indicated

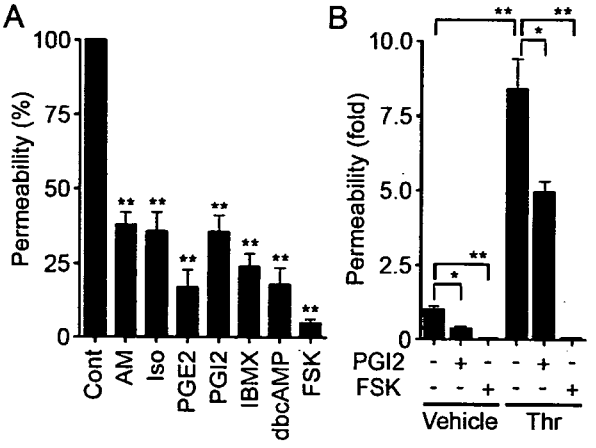

FIG. 1. cAMP enhances barrier function of monolayer VE cells. (A) Vascular permeability, reflecting barrier function, was analyzed by measuring the fluorescence of FITC-labeled dextran across the monolayer-cultured HUVECs as described in Materials and Methods. HUVECs grown on transwell filters were incubated with control (Cont), 0.1 μM AM, 200 μM Iso, 200-ng/ml PGE2, 10-μg/ml PGI2, 1 mM IBMX, 1 mM dbcAMP, and 10 μM FSK for 30 min. Average permeability ± standard deviation is expressed as a percentage compared to the control. (B) The effects of PGI2 and FSK on vascular permeability were quantified in the presence (+) or absence (−) (Vehicle) of 2 U of thrombin (Thr)/ml. Average permeability ± standard deviation is expressed as the increase relative to that observed in unstimulated HUVECs in the vehicle. Data shown are the results from at least three independent experiments. Significant differences from the control (A) or between two groups (B) determined by Student's *t* test are indicated by a single asterisk ($P < 0.05$) or double asterisks ($P < 0.01$).

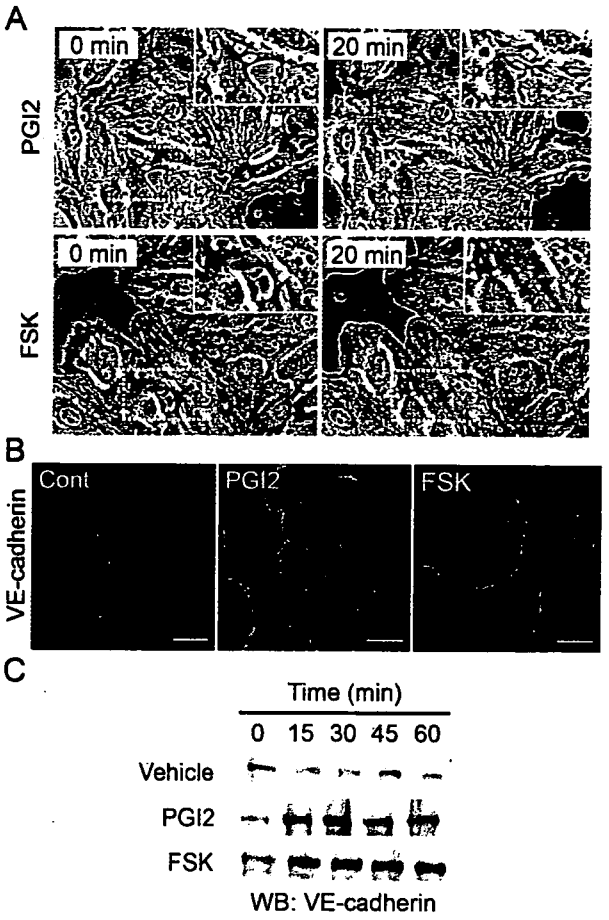

FIG. 2. cAMP induces AJ formation. (A) HUVECs cultured on a glass base dish were stimulated with 10 μg of PGI2/ml (upper panels) or with 10 μM FSK (lower panels) for 20 min and shown as phase-contrast images. Left and right panels show the cells before and after stimulation, respectively. The arrows indicate the sites of cell-cell contacts induced by PGI2 and FSK. The area boxed by the white broken line is enlarged in the right top of the panels. Bars, 50 μm. (B) Subconfluent HUVECs stimulated with vehicle (Cont), 10-μg/ml PGI2, and 10 μM FSK for 45 min were fixed, stained with anti-VE-cadherin antibody, and visualized with Alexa 488-conjugated secondary antibody through a confocal microscope (BX50WI; Olympus). Note that VE-cadherin (green) was accumulated at the cell-cell contact upon PGI2 and FSK stimulation. Bars, 50 μm. (C) Translocation of VE-cadherin was assessed by Triton X-100 solubility. HUVECs were stimulated with vehicle (top), 10-μg/ml PGI2 (middle), and 10 μM FSK (bottom) for the time indicated at the top and fractionated with cytoskeleton-stabilizing buffer as described in Materials and Methods. The Triton X-100-insoluble fraction was subjected to SDS-PAGE followed by Western blot analysis (WB) with anti-VE-cadherin.

agonists and drugs and lysed at 4°C in a pull-down lysis buffer (20 mM Tris-HCl [pH 7.5], 100 mM NaCl, 10 mM $MgCl_2$, 1% Triton X-100, 1 mM EGTA, 1 mM dithiothreitol, 1 mM Na_3VO_4, 1× protease inhibitor cocktail). GTP-bound Rap1 was collected on the GST-Rap1 binding domain of RalGDS precoupled to glutathione-Sepharose beads and subjected to SDS-PAGE followed by immunoblotting with anti-Rap1.

In vivo permeability assay. In vivo permeability was quantified by a modified Miles assay as described previously (29). In brief, ICR mice (Japan SLC, Inc.) shaved 3 days before experiments were lightly anesthetized and intravenously injected with 150 μl of 1% Evans blue dye solution (in saline) passed through a 0.22-μm-pore-size filter. Fifteen minutes later, 20 μl of PBS, VEGF (50 μg/ml), and/or 8-CPT-2′-O-Me-cAMP (1 mM) were applied by intradermal injections with a 30-gauge needle. The sites of intradermal injection were photographed 60 min after the injection, carefully dissected, and weighed. To quantify the vascular permeability, extravasated blue dye was eluted from the dissected skin with formamide at 56°C, and optical density was measured by spectrophotometry at 620 nm.

RESULTS

cAMP enhances the barrier property of monolayer-cultured endothelial cell. To evaluate the barrier function, we examined the permeability of FITC-labeled dextran across monolayer HUVECs. Expectedly, AM, Iso, PGE2, and PGI2 reduced basal endothelial permeability in HUVECs (Fig. 1A). PGI2 also reduced thrombin-induced vascular permeability (Fig. 1B). Other cAMP-elevating bio-ligands similarly reduced thrombin-induced permeability (data not shown). The bio-ligands for cAMP-elevating GPCR that we used in this study indeed increased cAMP in HUVECs (data not shown). Furthermore, IBMX (an inhibitor for phosphodiesterase), dbcAMP (a membrane-permeable cAMP analogue), and FSK (an adenylyl cyclase activator) resulted in a reduction of both basal and thrombin-induced endothelial permeability (Fig. 1; data not shown).

cAMP potentiates formation of AJ. Endothelial barrier function is largely dependent upon endothelial cell junctions. To investigate how cAMP affects AJ formation, we examined AJ organization by immunostaining with anti-VE-cadherin before and after stimulation. When subconfluent HUVECs with intercellular gaps were stimulated with PGI2 or FSK, the cells extended the plasma membrane and established cell-cell contacts with neighboring cells (Fig. 2A). Similar results were

obtained with AM and PGE2 (data not shown). Stimulation of HUVECs with PGI2 and FSK dramatically enhanced accumulation of VE-cadherin at cell-cell contacts (Fig. 2B).

The maturation of AJ requires homophilic binding of intercellular VE-cadherins and tight anchoring to the actin cytoskeleton via the cytoplasmic region through catenins. VE-cadherin anchored to the actin cytoskeleton is detected in detergent-insoluble fractions of cell lysates (26). We found an increase in VE-cadherin in the Triton X-100-insoluble fraction after stimulation with PGI2 or FSK (Fig. 2C). These results suggest that cAMP-elevating GPCR agonists potentiate AJ formation, which results in a cAMP-induced decrease in permeability.

cAMP promotes VE-cadherin-dependent endothelial cell adhesion. VE-cadherin is required for AJ formation (9). To test the involvement of a homophilic interaction of VE-cadherin in cAMP-enhanced AJ formation, we directly examined VE-cadherin-mediated cell adhesion. To mimic the VE-cadherin-dependent cell adhesion, we used VEC-Fc chimeric protein, which consisted of the extracellular domain of VE-cadherin fused to the Fc portion of immunoglobulin. HUVECs were plated onto VEC-Fc-coated dishes and time-lapse imaged. Cells attached within 5 min to the VEC-Fc-coated dish, subsequently spread, and exhibited a typical fried-egg morphology characterized by a large circular lamellipodium (Fig. 3A). No cells attached to the Fc-coated dish (Fig. 3B and C). Since cadherin-dependent cell adhesion requires Ca^{2+}, we examined the effect of Ca^{2+} chelation on cell adhesion to VEC-Fc-coated dishes. Cell adhesion to VEC-Fc-coated dishes was completely abolished by chelating extracellular Ca^{2+}, although cell attachment to the collagen-coated dish was unaffected (Fig. 3C and D). Basal and FSK-augmented cell adhesion to VEC-Fc-coated dishes was inhibited by EGTA (Fig. 3C). Both HUVECs and HAECs expressing VE-cadherin adhered to the VEC-Fc-coated dish (Fig. 3E). In clear contrast, HeLa and HEK293 cells, which express N-cadherin, but not VE-cadherin (20, 42), did not adhere to the VEC-Fc-coated dish, although these cells could attach to the collagen-coated dish (Fig. 3E; data not shown). Collectively, these results indicate that endothelial cell adhesion to the VEC-Fc-coated dish depends upon the homophilic ligation of VE-cadherin.

We proceeded to investigate the effect of cAMP-elevating GPCR agonists on VE-cadherin-mediated cell adhesion. The adhesion of HUVECs plated in the presence of PGI2 or FSK was evaluated by the alkaline phosphatase activity of remaining cells after washing. PGI2 enhanced adhesion of HUVECs to the VEC-Fc-coated dish in a concentration-dependent manner (Fig. 4A) and in a time-dependent manner (Fig. 4B). In a time course analysis, we noticed that enhanced adhesion was observed 7 min after the plating (Fig. 4B). Other cAMP-elevating GPCR agonists, including AM, Iso, and PGE2, potentiated VE-cadherin-dependent cell adhesion (Fig. 4C). In addition, similarly enhanced cell adhesion to the VEC-Fc-coated dish was also observed in the cells treated with cAMP-elevating drugs such as IBMX, dbcAMP, and FSK (Fig. 4F). Like PGI2, the effect of FSK on cell adhesion to the VEC-Fc-coated dish was concentration dependent and time dependent (Fig. 4D and E). This cAMP-induced cell adhesion to the VEC-Fc-coated dish depends on the enhanced homophilic ligation of VE-cadherin because FSK did not augment endothelial adhe-

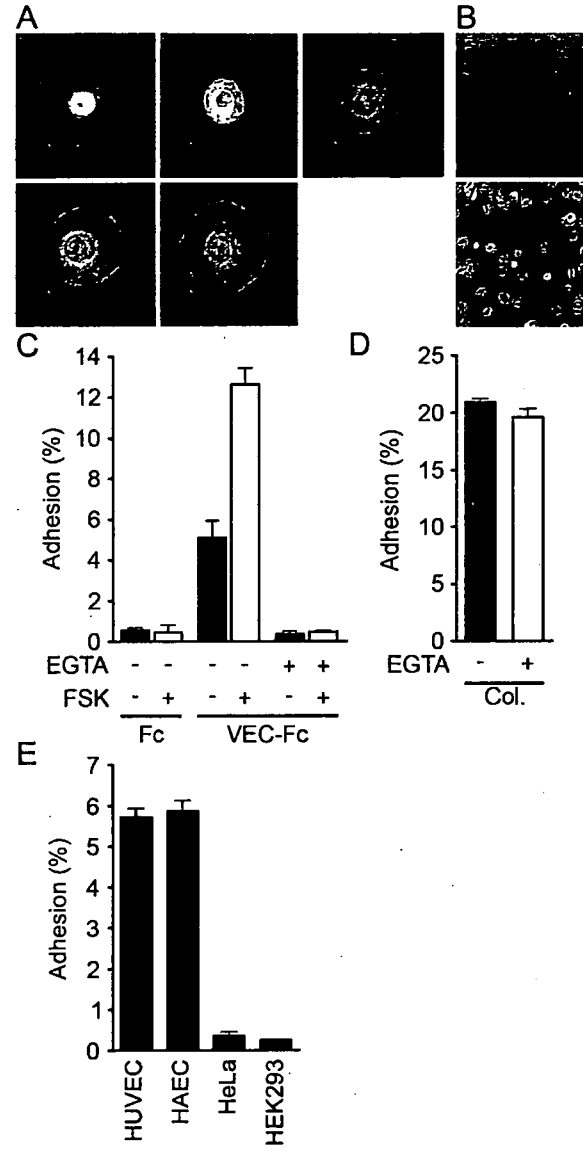

FIG. 3. Endothelial cells adhere to a VEC-Fc-coated dish through homophilic ligation of VE-cadherin. (A) HUVECs were plated onto the VEC-Fc-coated dish and time-lapse imaged at the time points (in minutes) indicated on the panels. Bar, 20 μM. (B) HUVECs were plated on the Fc-coated dish (top panel) or the VEC-Fc-coated dish (bottom panel) for 1 h and phase-contrast imaged after removal of nonadherent cells by washing with PBS-Ca/Mg. (C) HUVECs were plated onto either an Fc- or VEC-Fc-coated dish in the absence (−) or presence (+) of 5 mM EGTA and 10 μM FSK for 7 min. Cell adhesion was quantified as described in Materials and Methods. (D) Adhesion of HUVECs to a collagen-coated dish in the presence or absence of 5 mM EGTA was analyzed by a method similar to that described for panel C. (E) Adhesion of HUVECs, HAECs, and HeLa and HEK293 cells to the VEC-Fc-coated dish was examined as described in the legend for panel C. Cells adhering to the dishes of total input cells (percentage) is expressed as the mean ± standard deviation by measuring alkaline phosphatase activity of adherent cells divided by that of total input cells. Representative results from three independent experiments were shown in all panels.

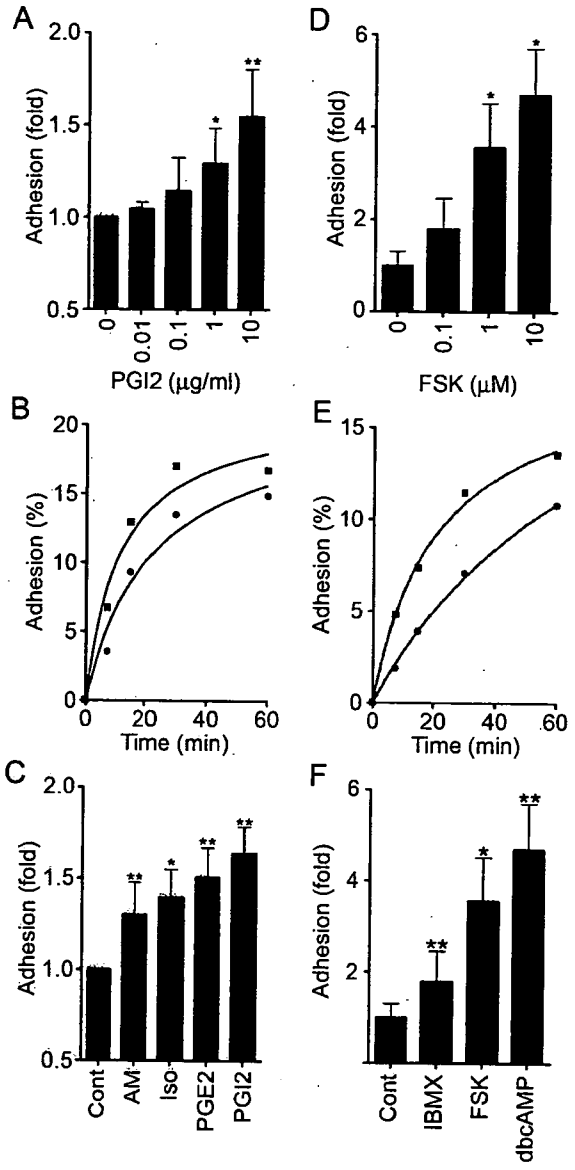

FIG. 4. cAMP potentiates VE-cadherin-dependent cell adhesion. (A) HUVECs were plated onto a VEC-Fc-coated dish in the presence of PGI2 at the concentrations indicated at the bottom for 7 min. Cell adhesion was quantified as described in Materials and Methods. Mean adhesion activity ± standard deviation is expressed as the increase compared with that observed in unstimulated cells. (B) HUVECs were plated onto the VEC-Fc-coated dish in the absence (circle) or presence (square) of 10-μg/ml PGI2 for the time indicated at the bottom. The percent adhesion was calculated by measuring the alkaline phosphatase activity of adherent cells divided by that of total input cells. (C) HUVECs stimulated with cAMP-elevating ligands similar to that described in the legend to panel A were assessed for adhesion activity. The concentration of stimulants was the same as described in the legend to Fig. 1A. (D) The effect of FSK on cell adhesion was analyzed by a method similar to that described for panel A, except that cells were preincubated for 10 min before plating. (E) The effect of 10 μM FSK on time-dependent adhesion was analyzed as described in the legend to panel B, except that cells were preincubated for 10 min before plating. (F) HUVECs stimulated with the reagent indicated at the same concentration used as described in the legend to Fig. 1A were analyzed for cell adhesion by a method similar to that described for panel D. Data are expressed as means ± standard deviations of the results from three independent experiments in panels A, C, D, and F. Representative results from three independent experiments were shown in panels B and E. A significant difference from the control determined by Student's t test is indicated with a single asterisk ($P < 0.05$) or double asterisks ($P < 0.01$).

sion to the Fc-coated dish or attachment to the VEC-Fc-coated dish in the absence of extracellular Ca^{2+} (Fig. 3C). These results indicate that cAMP potentiates VE-cadherin-dependent cell adhesion.

cAMP augments endothelial barrier function in a PKA-independent manner. PKA is suggested to be involved in cAMP-enhanced endothelial barrier function (43). Thus, we investigated the involvement of PKA in the regulation of endothelial barrier integrity by PGI2 and FSK. Unexpectedly, PGI2- and FSK-induced reduction of endothelial permeability was insensitive to a specific PKA inhibitor, H89 (7) (Fig. 5A and B). The reduction of thrombin-increased permeability by FSK was also unaffected by H89 (Fig. 5C). Consistently, H89 did not affect VE-cadherin-mediated cell adhesion enhancement by PGI2 and FSK (Fig. 5D and E). To confirm that H89 worked in HUVECs, we examined FSK-induced phosphorylation of CREB, a direct PKA substrate (38). Phosphorylation of CREB upon FSK stimulation was significantly inhibited by H89, indicating the effectiveness of this inhibitor in HUVECs (Fig. 5F). Therefore, these results apparently suggest a novel PKA-independent signaling pathway involved in cAMP-induced endothelial barrier function.

cAMP induces Rap1 activation. Besides PKA, Epac (cAMP-GEF) was identified as a novel cAMP target and a Rap1-specific GEF (5, 21). We therefore hypothesized that cAMP-activated Epac-Rap1 signaling is involved in the enhancement of VE-cadherin-dependent cell adhesion and endothelial barrier function. To address this possibility, we tested whether cAMP-elevating GPCR agonists induce Rap1 activation in HUVECs. Rap1 activity was determined by a pull-down assay by using a GST fusion protein of Rap1-binding domain of RalGDS according to the Bos's method. Bio-ligands for cAMP-elevating GPCR activated Rap1 (Fig. 6A). PGI2 rapidly induced Rap1 activation, which peaked at 1 to 5 min after the stimulation and then declined to the basal level by 10 min (Fig. 6C). A second wave of Rap1 activation was also observed 15 to 45 min after the stimulation (Fig. 6C). PGI2-induced Rap1 activation occurred in a concentration-dependent manner (Fig. 6B), which was associated with enhancement of VE-cadherin-dependent cell adhesion (Fig. 4A). Similarly, dbcAMP, FSK, and IBMX activated Rap1 (Fig. 6D). FSK-induced Rap1 activation reached a maximal level 2 to 5 min after the stimulation, and the level was sustained for up to 15 to 30 min (Fig. 6E). Collectively, these findings indicate that cAMP induces Rap1 activation in endothelial cells.

Specific activation of Epac reduces endothelial permeability and enhances VE-cadherin-dependent cell adhesion. To test whether the activation of endogenous Epac is sufficient to reduce endothelial permeability and to induce VE-cadherin-dependent cell adhesion, we used a recently developed cAMP analog, 8-CPT-2′-O-Me-cAMP, which specifically activates Epac without affecting PKA activity (13). As expected, 8-CPT-2′-O-Me-cAMP induced Rap1 activation in HUVECs (Fig. 7A), indicating that Epac is expressed in endothelial cells.

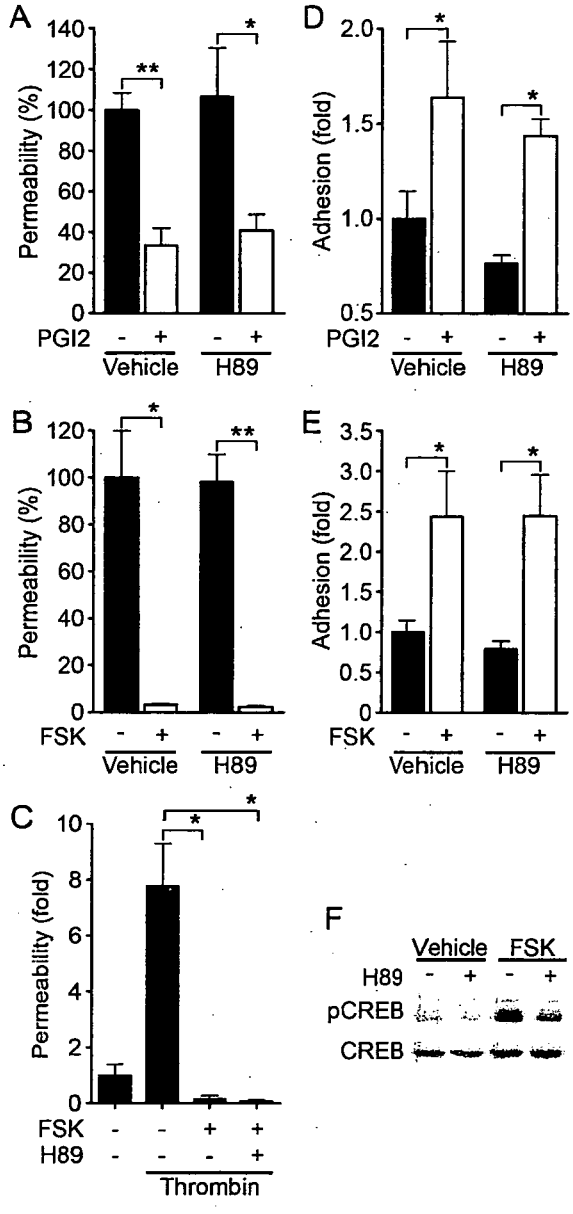

FIG. 5. cAMP-enhanced VE-cadherin-dependent cell adhesion and endothelial barrier function does not depend upon PKA. (A) Permeability across monolayer HUVECs grown on transwell filters were assessed by measuring FITC-labeled dextran as described in the legend to Fig. 1A. The effect of 10-μg/ml PGI2 on cell permeability without pretreatment (Vehicle) or with pretreatment with 5 μM H89, a specific PKA inhibitor, for 10 min is indicated as the percent permeability compared to that observed in untreated cells. +, present; −, absent. (B) The effect of 10 μM FSK on cell permeability without pretreatment (Vehicle) and with pretreatment with H89 was assessed similar to that described for panel A. (C) The effect of pretreatment of HUVECs with 5 μM H89 on FSK-induced reduction of 2-U/ml thrombin-induced permeability was analyzed. Permeability indicates the increase relative to that observed in untreated cells. (D) HUVECs untreated or pretreated with H89 for 10 min prior to stimulation with 10-μg/ml PGI2 were analyzed for cell adhesion as described in the legend to Fig. 4A. (E) HUVECs untreated or pretreated with H89 for 10 min prior to stimulation with 10 μM FSK were analyzed for cell adhesion as described in the legend to Fig. 4D. For panels A to E, data are expressed as means ± standard deviations of the results from triplicate samples. Similar results were obtained in at least three independent experiments. Significant differences between two groups determined by Student's t test are indicated by a single asterisk ($P < 0.05$) or double asterisks ($P < 0.01$). (F) HUVECs serum starved in 1% BSA-containing medium 199 for 6 h, followed by pretreatment with (+) or without (−) 5 μM H89 for 10 min, were stimulated with vehicle and 10 μM FSK for 10 min. Phosphorylation of CREB was assessed by Western blot analysis with anti-CREB (CREB) and anti-phospho-CREB-specific (pCREB) antibodies.

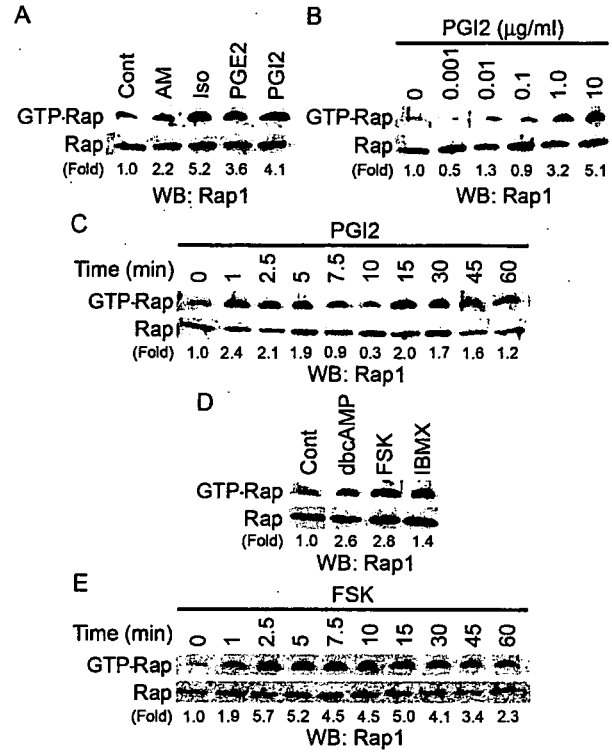

FIG. 6. cAMP induces Rap1 activation. (A) Serum-starved HUVECs kept in medium 199 containing 1% BSA overnight were stimulated with cAMP-elevating agonists for 2.5 min as indicated at the top and at the concentrations described in the legend to Fig. 1A. GTP-bound Rap1 was detected by pull-down assay as described in Materials and Methods. Activation indicates the ratio of the poststimulation GTP-Rap1 intensity of total Rap1 intensity to the prestimulation GTP-Rap1 intensity of total Rap1 intensity. (B) Rap1 activation was analyzed by detecting GTP-bound Rap1 with lysates from HUVECs stimulated with PGI2 for 2.5 min at the different concentrations indicated at the top. (C) Rap1 activation was analyzed by detecting GTP-bound Rap1 with lysates from cells stimulated with 10-μg/ml PGI2 for the time period indicated at the top. (D) Serum-starved HUVECs similar to those described in the legend to panel A were stimulated with the reagents indicated at the top for 10 min at the same concentrations described in the legend to Fig. 1A. Rap1 activation was assessed by a method similar to that described for panel A. (E) The effect of 10 μM FSK on time-dependent Rap1 activity was examined as described for panel C. Representative results from at least three independent experiments are shown for all panels.

8-CPT-2′-O-Me-cAMP dramatically reduced basal endothelial permeability, as did FSK and dbcAMP (Fig. 7B). Thrombin-induced permeability was also inhibited by 8-CPT-2′-O-Me-cAMP (Fig. 7C). Furthermore, we examined the effect of 8-CPT-2′-Me-cAMP on in vivo vascular permeability. VEGF-induced vascular permeability was completely blocked by coinjection of 8-CPT-2′-O-Me-cAMP (Fig. 7D). In addition, adhesion

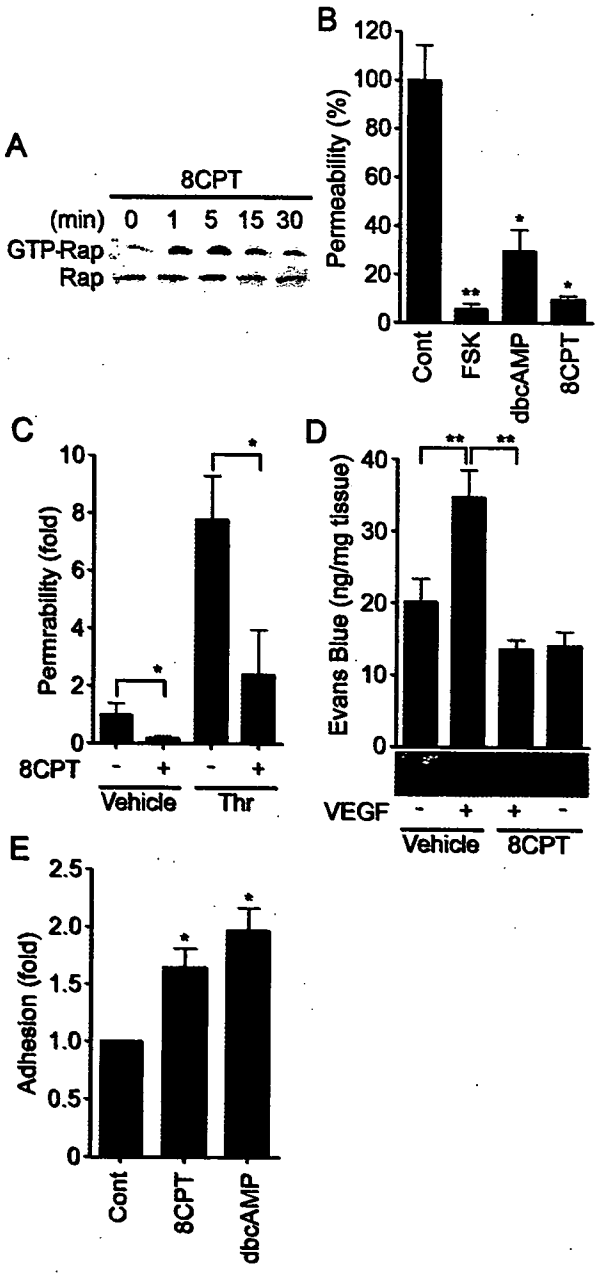

FIG. 7. Activation of Epac is sufficient to enhance VE-cadherin-dependent cell adhesion and endothelial barrier function. (A) Serum-starved HUVECs in medium 199 containing 1% BSA were stimulated with 0.2 mM 8-CPT-2′-O-Me-cAMP (8CPT) for the indicated time. Rap1 activity was determined as described in the legend to Fig. 6A. The result is a representative from three independent experiments. (B) Permeability of cells treated with the reagents as indicated on the bottom for 30 min was analyzed as described in the legend to Fig. 1A. (C) The effect of 0.2 mM 8CPT-2′-O-Me-cAMP on 2-U/ml thrombin-induced permeability was analyzed as described in the legend to Fig. 1B. (D) Effect of 8CPT-2′-O-Me-cAMP on VEGF-induced permeability was assessed by intradermal Miles assay as described in Materials and Methods. Amounts of extravasation of Evan blue in mouse dermal skin were measured 60 min after intradermal injection of vehicle and VEGF together with (+) or without (−) 8CPT. Mean leakage ± standard deviation of the results from 6 mice per group is expressed as nanograms of weight of extravasated Evans blue per milligram of weight of dermal skin. A photograph on the bottom shows leakage of Evans blue in dermal skin. (E) HUVEC adhesion to the VEC-Fc-coated dish in the presence of 0.2 mM 8CPT and 1 mM dbcAMP for 7 min was analyzed as described in the legend to Fig. 4F. In panels B, C, and E, data are expressed as means ± standard deviations of the results from triplicate samples. A significant difference from the control in panels B and E or between two groups in panels C and D was determined by Student's t test and indicated by a single asterisk ($P < 0.05$) or double asterisks ($P < 0.01$).

of HUVECs to the VEC-Fc-coated dish was significantly enhanced by 8-CPT-2′-O-Me-cAMP (Fig. 7E). Hence, Epac activation is sufficient to enhance VE-cadherin-dependent cell adhesion and to augment endothelial barrier function in vitro and in vivo.

Rap1 activation is essential for VE-cadherin-dependent cell adhesion and endothelial barrier function. We next proceeded to investigate the role of Rap1 in VE-cadherin-dependent cell adhesion and endothelial barrier function. To examine the effect of Rap1 on cell permeability and VE-cadherin-mediated cell adhesion, we inactivated endogenous Rap1 by adenovirus-expressing Rap1GAPII (Ad-RapGAP), which specifically catalyzes the hydrolysis of GTP to GDP on Rap1 (30). As shown in Fig. 8A, endogenous Rap1 activity was almost completely suppressed by the expression of increasing amounts of Rap1GAPII in HUVECs. This Rap1 inactivation paralleled the increase in basal permeability (Fig. 8B) and the inhibition of cell adhesion to the VEC-Fc-coated dish (Fig. 8D). In contrast, a constitutively active Rap1, Rap1V12, reduced both basal and thrombin-increased cell permeability (Fig. 8C). VE-cadherin-mediated cell adhesion was also enhanced by Rap1V12 and EpacΔcAMP, a constitutively active mutant of Epac (Fig. 8D). Taken together, these results indicate that Rap1 activation is required for VE-cadherin-mediated cell adhesion and endothelial barrier function.

cAMP enhances VE-cadherin-dependent cell adhesion and endothelial barrier function by activating Rap1. To test the requirement for Rap1 in endothelial barrier enhancement by cAMP-elevating GPCR agonists, we infected HUVECs with Ad-RapGAP and examined the effect of inactivation of Rap1 on PGI2- and FSK-induced reduction of cell permeability. Although basal endothelial permeability was reduced by PGI2 and FSK (Fig. 9A and B), overexpression of Rap1GAPII increased not only basal but also PGI2- and FSK-reduced endothelial permeability, indicating the requirement of Rap1 activity for PGI2- and FSK-induced barrier enhancement. We also investigated the involvement of Rap1 in PGI2- and FSK-induced VE-cadherin-dependent cell adhesion. PGI2 and FSK augmented VE-cadherin-dependent cell adhesion of HUVECs infected with control adenovirus (Ad-LacZ); however, their effects were dramatically suppressed by overexpression of Rap1GAPII (Fig. 9C and D). These data demonstrate that cAMP enhances VE-cadherin-dependent cell adhesion and endothelial barrier functions by activating Rap1.

cAMP induces endothelial cortical actin rearrangement in a Rap1-dependent manner. Endothelial barrier function is largely dependent upon the actin cytoskeleton supporting junctional adhesion molecules (10). Thus, we examined the effect of cAMP on cortical actin polymerization and assembly of polymerized actin in a monolayer of endothelial cells. Cortactin, an actin-binding protein, is known to be implicated in cortical actin rearrangement (8) and suggested to regulate S1P-induced endothelial barrier enhancement (11). PGI2,

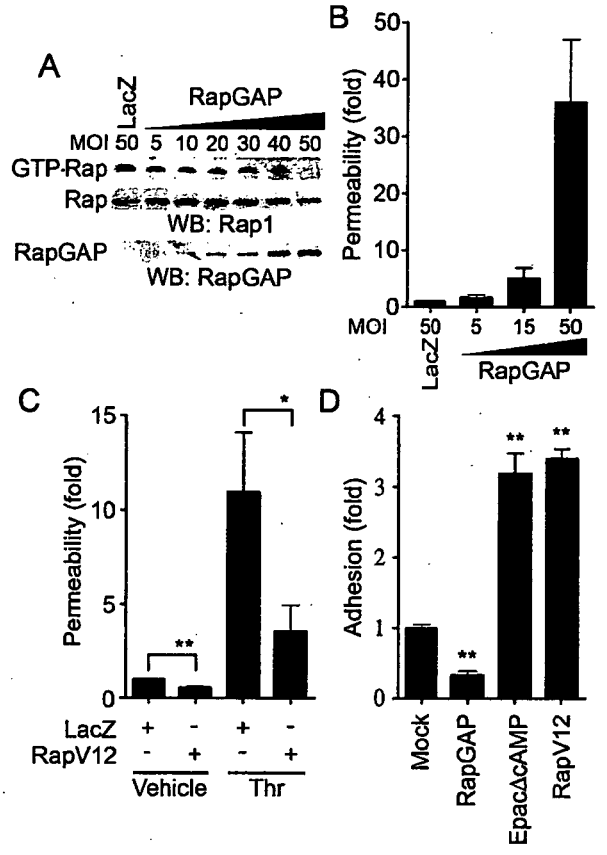

FIG. 8. Rap1 plays a critical role in VE-cadherin-dependent cell adhesion and endothelial barrier function. (A) Rap1 inactivation was assessed by detecting GTP-Rap1 in HUVECs infected with different MOI of adenovirus-expressing Rap1GAPII (RapGAP) as indicated at the top. An adenovirus-expressing LacZ at an MOI of 50 was used as a control. GTP-bound Rap1 (GTP-Rap) was detected by pull-down assay as described in Materials and Methods. Rap1 (Rap) and Rap1GAPII (RapGAP) expression were examined by Western blot analysis. (B) The permeability of FITC-dextran across HUVECs infected with adenovirus as indicated at the bottom was analyzed as described in Materials and Methods. Data are the means ± standard deviations of the results from three independent experiments and are expressed as increases relative to those of LacZ-infected cells. (C) Monolayer HUVECs infected with either an adenovirus-expressing LacZ or that expressing Rap1V12 at an MOI of 50 for 24 h were medium changed and cultured for another 24 h. The permeability of cells upon 2-U/ml thrombin stimulation (Thr) after starvation for 1 h was analyzed as described in the legend to Fig. 1B. Data are the means ± standard deviations of the results from five independent experiments and are expressed as inductions relative to those of untreated HUVECs infected with the LacZ-expressing virus. (D) HUVECs were transfected with either empty vector (Mock), plasmids expressing Rap1GAPII (RapGAP), EpacΔcAMP, or Rap1V12 together with the luciferase reporter construct. Transfected cells were plated on the VEC-Fc-coated dish and allowed to adhere for 15 min. Cell adhesion was analyzed as described in Materials and Methods. Data are expressed as increases compared to those of mock-transfected cells. The results indicate the means ± standard deviations of the results from triplicate samples. Similar results were obtained in three independent experiments. Significant differences between two groups in panel C or from the control in panel D are determined by Student's *t* test and are indicated by a single asterisk ($P < 0.05$) or double asterisks ($P < 0.01$).

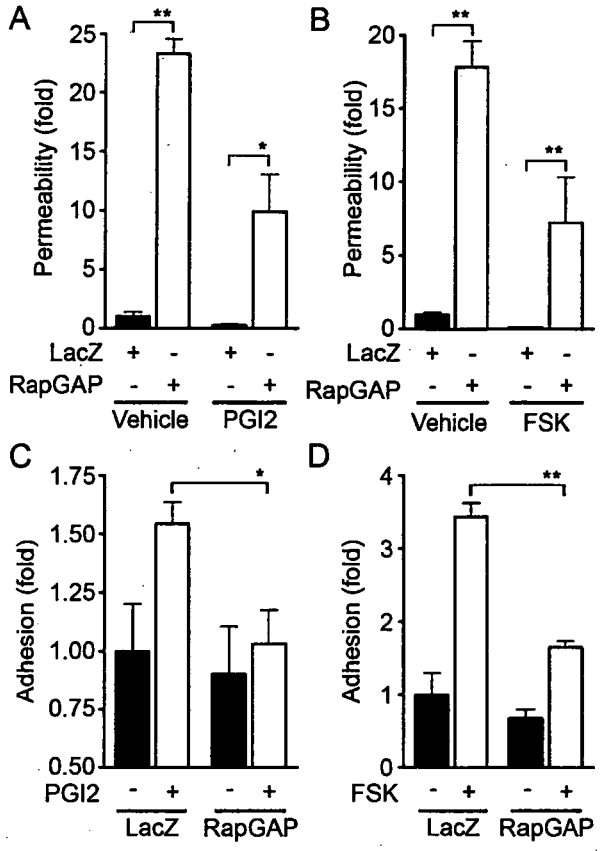

FIG. 9. Inactivation of Rap1 reduces PGI2- and FSK-induced barrier function and VE-cadherin-mediated cell adhesion. (A) Monolayer-cultured HUVECs grown on transwell filters were infected with either LacZ-expressing adenovirus (Ad-LacZ) or Rap1GAPII-expressing virus (Ad-RapGAP) at an MOI of 40 for 24 h. Medium was replaced with fresh medium after infection. Cells were cultured for an additional 24 h and treated with 10 μg of PGI2/ml for 30 min after serum starvation for 1 h. Permeability was analyzed as described in Materials and Methods. (B) The effect of 10 μM FSK on permeability in HUVECs infected with Ad-RapGAP was similarly analyzed. (C) HUVECs were infected with either Ad-LacZ or Ad-RapGAP at an MOI of 40 for 24 h. HUVECs resuspended in medium 199 with 0.5% BSA were plated onto VEC-Fc-coated dishes in the presence (+) or absence (−) of 10 μg of PGI2/ml for 7 min. Cell adhesion activity was quantified as described in the legend to Fig. 4A. (D) The effect of FSK on adhesion of HUVECs infected with Ad-RapGAP was analyzed similarly to that described for panel C. Resuspended HUVECs were preincubated with 10 μM FSK for 10 min before plating. Significant differences between two groups determined by Student's *t* test are indicated by a single asterisk ($P < 0.05$) or double asterisks ($P < 0.01$).

FSK, and 8-CPT-2′-O-Me-cAMP dramatically induced accumulation of polymerized actin and cortactin at cell-cell contacts (Fig. 10A). To explore the involvement of Rap1 in cAMP-mediated cortical actin rearrangement, an expression vector encoding Rap1GAPII was introduced into endothelial cells. FSK enhanced actin polymerization at cell-cell contacts in cells transfected with control vector encoding EGFP, whereas it did not in cells expressing Rap1GAPII (Fig. 10B). Cytochalasin D, an actin-depolymerizing agent, attenuated FSK-induced barrier enhancement (Fig. 10C) and inhibited FSK-induced VE-cadherin-dependent cell adhesion (Fig. 10D). These results suggest that the cortical actin rearrangement promoted by

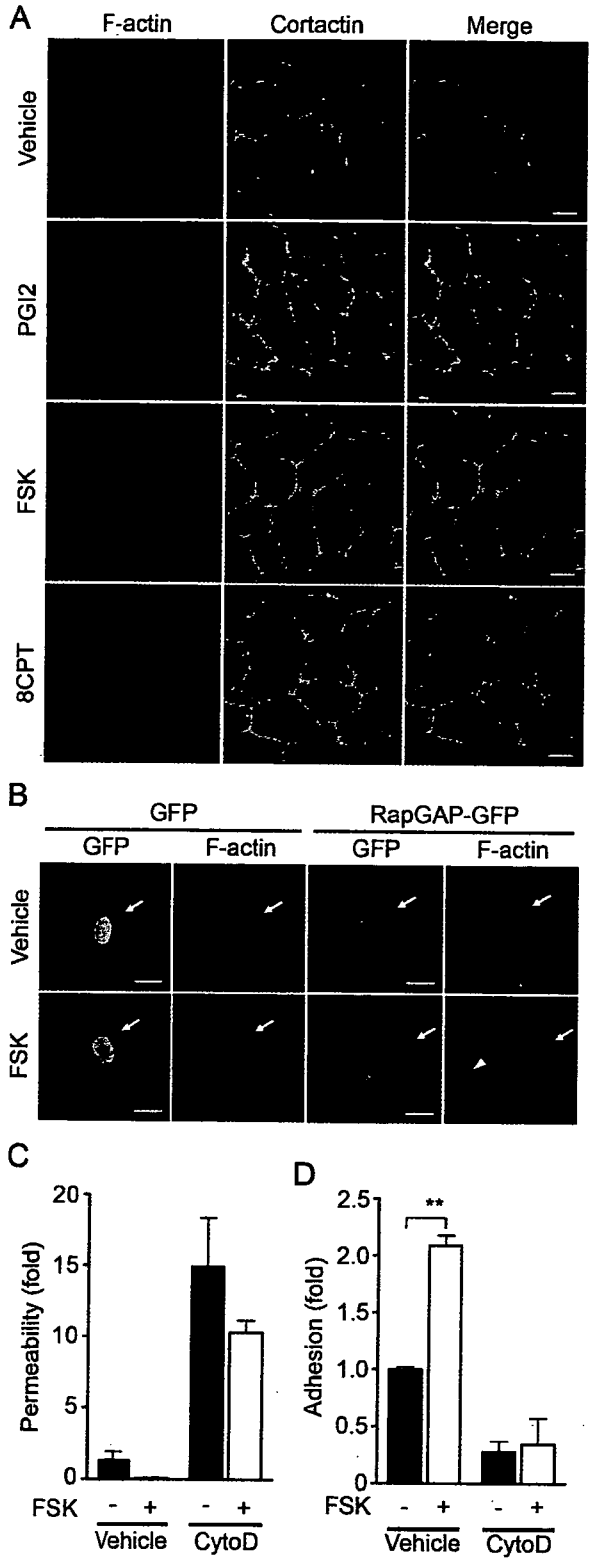

FIG. 10. cAMP induces cortical actin rearrangement in a Rap1-dependent manner. (A) Monolayer-cultured HUVECs starved in 0.5% BSA-containing medium 199 for 3 h were stimulated with vehicle (top row), 10-μg/ml PGI2 (second row), 10 μM FSK (third row), and 0.2 mM 8-CPT-2′-O-Me-cAMP (8CPT) (bottom row) for 30 min. Fixed and permeabilized cells were stained with rhodamine-phalloidin (left column) and with anti-cortactin (center column). Rhodamine images to detect F-actin (red) and Alexa 488 images for cortactin visualized by Alexa 488-labeled secondary antibody (green) were obtained through a confocal microscope (BX50WI). Right panels show the merged images of rhodamine and Alexa 488 images. Bars, 20 μm. (B) HUVECs transfected with an EGFP-expressing vector (left) and pCXN2-Rap1GAPII-IRES-EGFP (right) were serum starved in 0.5% BSA-containing medium 199 for 3 h and stimulated with vehicle (top panels) and 10 μM FSK (bottom panels). Cells were fixed, permeabilized, and stained with Rhodamine-phalloidin. EGFP images (green) and rhodamine images showing F-actin (red) were obtained similar to those in panel A. Arrows and arrowhead indicate transfected and untransfected cells, respectively. Bars, 20 μm. (C) Cell permeability of HUVECs pretreated with 2 μM cytochalasin D (CytoD) for 30 min followed by 10 μM FSK stimulation for 30 min was analyzed as described in the legend to Fig. 1A. −, absent; +, present. (D) The effect of pretreatment of 2 μM cytochalasin D (CytoD) on adhesion of HUVECs stimulated with FSK was analyzed as described in the legend to Fig. 5E. A significant difference between two groups determined by Student's t test is indicated by double asterisks ($P < 0.01$).

cAMP-Epac-Rap1 signaling may contribute to the potentiation of endothelial barrier function and VE-cadherin-dependent cell adhesion.

DISCUSSION

cAMP is a well-known intracellular signaling molecule that is capable of restoring diminished endothelial barrier function. Previous reports suggested that cAMP-induced barrier enhancement occurs through PKA (27, 39). In this study, however, we demonstrated a novel PKA-independent signaling pathway, the cAMP-Epac-Rap1 signaling pathway, involved in cAMP-induced barrier function based on the following observations. PGI2- and FSK-reduced endothelial permeability was insensitive to H89. A specific activator for Epac, 8-CPT-2′-O-Me-cAMP, reduced both basal and thrombin-increased permeability. Plasma leakage in response to VEGF was also inhibited by 8-CPT-2′-O-Me-cAMP in vivo. We found that the activation of Rap1 leads to decreased permeability. Not only all cAMP-elevating bio-ligands we tested but also FSK, db-cAMP, and IBMX activated Rap1. Consistently, cAMP-dependent Rap1 activation upon stimulation by these ligands involved Epac in the regulation of barrier function. A previous report showed that Rap1 is phosphorylated by PKA in neutrophils and platelets, although the function of phosphorylated Rap1 has not been elucidated (37). So far, Epac is known to regulate several biological functions including integrin-dependent cell adhesion, insulin secretion, and calcium release through ryanodine-sensitive Ca^{2+} channels (reviewed in reference 5). In addition to these Epac-mediated functions, we show, for the first time, that Epac-Rap1 signaling is important for regulation of endothelial barrier function.

AJ assembly contributes to the regulation of barrier function. Rap1 is involved in the formation and maintenance of AJ constituted by cadherin (23, 41). Recently, it has been reported that homophilic ligation of E-cadherin induced Rap1 activation, which may be responsible for maturation of AJ (20). Consistently, suppression of endogenous Rap1 inhibits formation of E-cadherin-dependent cell adhesion (36), suggesting the critical role of Rap1 in the establishment of cadherin-based cell-cell contacts. Here, we demonstrate that Rap1 also acts downstream of cAMP-Epac to potentiate VE-cadherin-depen-

dent cell adhesion, thereby improving barrier function. In addition to cAMP-elevating ligands, S1P, which enhances AJ formation and barrier function (18, 26), also activated Rap1 (our unpublished data). Thus, Rap1 may play a crucial role in barrier function induced by various types of barrier-improving factors.

Our data and previous studies show that cAMP protects thrombin-induced endothelial barrier dysfunction. cAMP does not limit the effect of thrombin on the initial loss of endothelial barrier (32). Instead, cAMP enhances the restoration of barrier function disrupted by thrombin. Recently, it was also reported that Cdc42 regulates the restoration of endothelial barrier function disrupted by thrombin (24). Thus, cAMP-Epac-Rap1 signaling may facilitate the formation of VE-cadherin-based cell-cell contacts, cooperatively or in parallel with Cdc42.

Rap1 enhances integrin-dependent cell adhesion in a variety of hematopoietic cells by modulating the affinity and avidity of integrin (6, 22). Cell adhesion to VEC-Fc-coated dishes was augmented by Rap1 activation, suggesting that the homophilic binding of VE-cadherin is also likely ascribed to the affinity and avidity of VE-cadherin modulated by Rap1-triggered inside out signaling. Hogan et al. reported that Rap1 activity is required for the targeting of E-cadherin molecules into nascent cell-cell contact sites, which in turn leads to the maturation of E-cadherin-based cell-cell contacts (20). Thus, cAMP-Epac-Rap1 signaling may also regulate the recruitment of VE-cadherin into maturing cell-cell contacts. Since downstream signaling of Rap1 that increases homophilic binding of VE-cadherin has not yet been characterized, the effector of cAMP-Epac-Rap1 signaling will need to be identified.

The actin cytoskeleton is a critical determinant of vascular integrity (10). PGI2, FSK, and 8-CPT-2′-O-Me-cAMP induced cortical actin rearrangement in a Rap1-dependent manner. FSK-induced VE-cadherin-dependent cell adhesion was inhibited by cytochalasin D. Thus, Rap1 may promote VE-cadherin-dependent cell adhesion by inducing cortical actin rearrangement. AF-6 may act downstream of Rap1 to regulate the actin cytoskeleton, since it binds to GTP-bound Rap1 and the actin cytoskeleton regulator, profilin, and is localized at AJ (2). Consistently, Canoe, the drosophila homolog of AF-6, and Rap1 function in the same molecular pathway during embryonic dorsal closure, which requires cell-cell contacts (3). S1P promotes endothelial barrier function by inducing Rac-dependent cortical actin rearrangement. S1P also induces Rap1 activation (our unpublished data). A previous report indicates that Rac can function downstream of Rap1 in the processing of the amyloid precursor protein (28). Taken together, Rac may act downstream of Rap1 to induce cortical actin rearrangement.

In conclusion, we have demonstrated that the cAMP-Epac-Rap1 signaling pathway promotes VE-cadherin-mediated cell adhesion and consequently improves endothelial barrier function.

ACKNOWLEDGMENTS

We thank J. L. Bos and W. A. Muller for plasmids, M. Matsuda and S. Hattori for adenovirus, J. T. Pearson for critical reading, and M. Sone, K. Yamamoto, and N. Irisawa for technical assistance.

This work was supported by grants from the Ministry of Health, Labor, and Welfare of Japan, from the Promotion of Fundamental Studies in Health Science of the Organization for Pharmaceutical Safety and Research of Japan, from the Ministry of Education, Science, Sports, and Culture of Japan, from the Uehara Memorial Foundation, and from Senri Life Science Foundation.

REFERENCES

1. **Andriopoulou, P., P. Navarro, A. Zanetti, M. G. Lampugnani, and E. Dejana.** 1999. Histamine induces tyrosine phosphorylation of endothelial cell-to-cell adherens junctions. Arterioscler. Thromb. Vasc. Biol. **19**:2286–2297.
2. **Boettner, B., E. E. Govek, J. Cross, and L. Van Aelst.** 2000. The junctional multidomain protein AF-6 is a binding partner of the Rap1A GTPase and associates with the actin cytoskeletal regulator profilin. Proc. Natl. Acad. Sci. USA **97**:9064–9069.
3. **Boettner, B., P. Harjes, S. Ishimaru, M. Heke, H. Q. Fan, Y. Qin, L. Van Aelst, and U. Gaul.** 2003. The AF-6 homolog canoe acts as a Rap1 effector during dorsal closure of the Drosophila embryo. Genetics **165**:159–169.
4. **Bogatcheva, N. V., J. G. Garcia, and A. D. Verin.** 2002. Molecular mechanisms of thrombin-induced endothelial cell permeability. Biochemistry (Moscow) **67**:75–84.
5. **Bos, J. L.** 2003. Epac: a new cAMP target and new avenues in cAMP research. Nat. Rev. Mol. Cell Biol. **4**:733–738.
6. **Bos, J. L., J. de Rooij, and K. A. Reedquist.** 2001. Rap1 signalling: adhering to new models. Nat. Rev. Mol. Cell Biol. **2**:369–377.
7. **Chijiwa, T., A. Mishima, M. Hagiwara, M. Sano, K. Hayashi, T. Inoue, K. Naito, T. Toshioka, and H. Hidaka.** 1990. Inhibition of forskolin-induced neurite outgrowth and protein phosphorylation by a newly synthesized selective inhibitor of cyclic AMP-dependent protein kinase, N-[2-(p-bromocinnamylamino)ethyl]-5-isoquinolinesulfonamide (H-89), of PC12D pheochromocytoma cells. J. Biol. Chem. **265**:5267–5272.
8. **Daly, R. J.** 2004. Cortactin signalling and dynamic actin networks. Biochem. J. **382**:13–25. [Online.] doi:10.1042/BJ20040737.
9. **Dejana, E.** 2004. Endothelial cell-cell junctions: happy together. Nat. Rev. Mol. Cell Biol. **5**:261–270.
10. **Dudek, S. M., and J. G. Garcia.** 2001. Cytoskeletal regulation of pulmonary vascular permeability. J. Appl. Physiol. **91**:1487–1500.
11. **Dudek, S. M., J. R. Jacobson, E. T. Chiang, K. G. Birukov, P. Wang, X. Zhan, and J. G. Garcia.** 2004. Pulmonary endothelial cell barrier enhancement by sphingosine 1-phosphate: roles for cortactin and myosin light chain kinase. J. Biol. Chem. **279**:24692–24700.
12. **Endo, A., K. Nagashima, H. Kurose, S. Mochizuki, M. Matsuda, and N. Mochizuki.** 2002. Sphingosine 1-phosphate induces membrane ruffling and increases motility of human umbilical vein endothelial cells via vascular endothelial growth factor receptor and CrkII. J. Biol. Chem. **277**:23747–23754.
13. **Enserink, J. M., A. E. Christensen, J. de Rooij, M. van Triest, F. Schwede, H. G. Genieser, S. O. Doskeland, J. L. Blank, and J. L. Bos.** 2002. A novel Epac-specific cAMP analogue demonstrates independent regulation of Rap1 and ERK. Nat. Cell Biol. **4**:901–906.
14. **Esser, S., M. G. Lampugnani, M. Corada, E. Dejana, and W. Risau.** 1998. Vascular endothelial growth factor induces VE-cadherin tyrosine phosphorylation in endothelial cells. J. Cell Sci. **111**(Pt 13):1853–1865.
15. **Farmer, P. J., S. G. Bernier, A. Lepage, G. Guillemette, D. Regoli, and P. Sirois.** 2001. Permeability of endothelial monolayers to albumin is increased by bradykinin and inhibited by prostaglandins. Am. J. Physiol. Lung Cell. Mol. Physiol. **280**:L732–L738.
16. **Fukuhara, S., M. J. Marinissen, M. Chiariello, and J. S. Gutkind.** 2000. Signaling from G protein-coupled receptors to ERK5/Big MAPK 1 involves Galpha q and Galpha 12/13 families of heterotrimeric G proteins. Evidence for the existence of a novel Ras AND Rho-independent pathway. J. Biol. Chem. **275**:21730–21736.
17. **Gamble, J. R., J. Drew, L. Trezise, A. Underwood, M. Parsons, L. Kasminkas, J. Rudge, G. Yancopoulos, and M. A. Vadas.** 2000. Angiopoietin-1 is an antipermeability and anti-inflammatory agent in vitro and targets cell junctions. Circ. Res. **87**:603–607.
18. **Garcia, J. G., F. Liu, A. D. Verin, A. Birukova, M. A. Dechert, W. T. Gerthoffer, J. R. Bamberg, and D. English.** 2001. Sphingosine 1-phosphate promotes endothelial cell barrier integrity by Edg-dependent cytoskeletal rearrangement. J. Clin. Investig. **108**:689–701.
19. **Hippenstiel, S., M. Witzenrath, B. Schmeck, A. Hocke, M. Krisp, M. Krull, J. Seybold, W. Seeger, W. Rascher, H. Schutte, and N. Suttorp.** 2002. Adrenomedullin reduces endothelial hyperpermeability. Circ. Res. **91**:618–625.
20. **Hogan, C., N. Serpente, P. Cogram, C. R. Hosking, C. U. Bialucha, S. M. Feller, V. M. M. Braga, W. Birchmeier, and Y. Fujita.** 2004. Rap1 regulates the formation of E-cadherin-based cell-cell contacts. Mol. Cell. Biol. **24**:6690–6700.
21. **Kawasaki, H., G. M. Springett, N. Mochizuki, S. Toki, M. Nakaya, M. Matsuda, D. E. Housman, and A. M. Graybiel.** 1998. A family of cAMP-binding proteins that directly activate Rap1. Science **282**:2275–2279.
22. **Kinbara, K., L. E. Goldfinger, M. Hansen, F. L. Chou, and M. H. Ginsberg.**

2003. Ras GTPases: integrins' friends or foes? Nat. Rev. Mol. Cell Biol. 4:767–776.
23. **Knox, A. L., and N. H. Brown.** 2002. Rap1 GTPase regulation of adherens junction positioning and cell adhesion. Science 295:1285–1288.
24. **Konklis, P., M. Konstantoulaki, S. Vogel, M. Broman, and A. B. Malik.** 2004. Cdc42 regulates the restoration of endothelial barrier function. Circ. Res. 94:159–166.
25. **Langeler, E. G., and V. W. van Hinsbergh.** 1991. Norepinephrine and iloprost improve barrier function of human endothelial cell monolayers: role of cAMP. Am. J. Physiol. 260:C1052–C1059.
26. **Lee, M. J., S. Thangada, K. P. Claffey, N. Ancellin, C. H. Liu, M. Kluk, M. Volpi, R. I. Sha'afi, and T. Hla.** 1999. Vascular endothelial cell adherens junction assembly and morphogenesis induced by sphingosine-1-phosphate. Cell 99:301–312.
27. **Lum, H., H. A. Jaffe, I. T. Schulz, A. Masood, A. RayChaudhury, and R. D. Green.** 1999. Expression of PKA inhibitor (PKI) gene abolishes cAMP-mediated protection to endothelial barrier dysfunction. Am. J. Physiol. 277: C580–C588.
28. **Maillet, M., S. J. Robert, M. Cacquevel, M. Gastineau, D. Vivien, J. Bertoglio, J. L. Zugaza, R. Fischmeister, and F. Lezoualc'h.** 2003. Crosstalk between Rap1 and Rac regulates secretion of sAPPalpha. Nat. Cell Biol. 5:633–639.
29. **Miles, A. A., and E. M. Miles.** 1952. Vascular reactions to histamine, histamine-liberator and leukotaxine in the skin of guinea-pigs. J. Physiol. 118: 228–257.
30. **Mochizuki, N., Y. Ohba, E. Kiyokawa, T. Kurata, T. Murakami, T. Ozaki, A. Kitabatake, K. Nagashima, and M. Matsuda.** 1999. Activation of the ERK/MAPK pathway by an isoform of rap1GAP associated with G alpha(i). Nature 400:891–894.
31. **Mori, Y., T. Nishikimi, N. Kobayashi, H. Ono, K. Kangawa, and H. Matsuoka.** 2002. Long-term adrenomedullin infusion improves survival in malignant hypertensive rats. Hypertension 40:107–113.
32. **Moy, A. B., J. E. Bodmer, K. Blackwell, S. Shasby, and D. M. Shasby.** 1998. cAMP protects endothelial barrier function independent of inhibiting MLC20-dependent tension development. Am. J. Physiol. 274:L1024–L1029.
33. **Navarro, P., L. Ruco, and E. Dejana.** 1998. Differential localization of VE- and N-cadherins in human endothelial cells: VE-cadherin competes with N-cadherin for junctional localization. J. Cell Biol. 140:1475–1484.
34. **Ohba, Y., K. Ikuta, A. Ogura, J. Matsuda, N. Mochizuki, K. Nagashima, K. Kurokawa, B. J. Mayer, K. Maki, J. Miyazaki, and M. Matsuda.** 2001. Requirement for C3G-dependent Rap1 activation for cell adhesion and embryogenesis. EMBO J. 20:3333–3341.
35. **Parandoosh, Z., C. A. Bogowitz, and M. P. Nova.** 1998. A fluorometric assay for the measurement of endothelial cell density in vitro. In Vitro Cell. Dev. Biol. Anim. 34:772–776.
36. **Price, L. S., A. Hajdo-Milasinovic, J. Zhao, F. J. Zwartkruis, J. G. Collard, and J. L. Bos.** 2004. Rap1 regulates E-cadherin-mediated cell-cell adhesion. J. Biol. Chem. 279:35127–35132.
37. **Quilliam, L. A., H. Mueller, B. P. Bohl, V. Prossnitz, L. A. Sklar, C. J. Der, and G. M. Bokoch.** 1991. Rap1A is a substrate for cyclic AMP-dependent protein kinase in human neutrophils. J. Immunol. 147:1628–1635.
38. **Shaywitz, A. J., and M. E. Greenberg.** 1999. CREB: a stimulus-induced transcription factor activated by a diverse array of extracellular signals. Annu. Rev. Biochem. 68:821–861.
39. **Stelzner, T. J., J. V. Weil, and R. F. O'Brien.** 1989. Role of cyclic adenosine monophosphate in the induction of endothelial barrier properties. J. Cell. Physiol. 139:157–166.
40. **Ukropec, J. A., M. K. Hollinger, S. M. Salva, and M. J. Woolkalis.** 2000. SHP2 association with VE-cadherin complexes in human endothelial cells is regulated by thrombin. J. Biol. Chem. 275:5983–5986.
41. **Yajnik, V., C. Paulding, R. Sordella, A. I. McClatchey, M. Saito, D. C. Wahrer, P. Reynolds, D. W. Bell, R. Lake, S. van den Heuvel, J. Settleman, and D. A. Haber.** 2003. DOCK4, a GTPase activator, is disrupted during tumorigenesis. Cell 112:673–684.
42. **Yano, H., Y. Mazaki, K. Kurokawa, S. K. Hanks, M. Matsuda, and H. Sabe.** 2004. Roles played by a subset of integrin signaling molecules in cadherin-based cell-cell adhesion. J. Cell Biol. 166:283–295.
43. **Yuan, S. Y.** 2002. Protein kinase signaling in the modulation of microvascular permeability. Vascul. Pharmacol. 39:213–223.

THE JOURNAL OF BIOLOGICAL CHEMISTRY

Vol. 280, No. 6, Issue of February 11, pp. 5022–5031, 2005
Printed in U.S.A.

Local Activation of Rap1 Contributes to Directional Vascular Endothelial Cell Migration Accompanied by Extension of Microtubules on Which RAPL, a Rap1-associating Molecule, Localizes*[S]

Received for publication, August 24, 2004, and in revised form, November 23, 2004
Published, JBC Papers in Press, November 29, 2004, DOI 10.1074/jbc.M409701200

Hisakazu Fujita, Shigetomo Fukuhara, Atsuko Sakurai, Akiko Yamagishi, Yuji Kamioka, Yoshikazu Nakaoka, Michitaka Masuda, and Naoki Mochizuki‡

From the Department of Structural Analysis, National Cardiovascular Center Research Institute, Suita, Osaka 565-8565, Japan

Endothelial cell migration is promoted by chemoattractants and is accompanied with microtubule extension toward the leading edge. Cytoskeletal microtubules polarize to function as rails for delivering a variety of molecules by motor proteins during cell migration. It remains, however, unclear how directional migration with polarized extension of microtubules is regulated. Here we report that Rap1 controls the migration of vascular endothelial cells. We found that Rap1-associating molecule, RAPL, which belongs to the Ras association domain family (Rassf), localized on microtubules and that activated Rap1 induced dissociation of RAPL from microtubules. A Rap1 activation-monitoring probe based on the fluorescence resonance energy transfer enabled us to demonstrate that local Rap1 activation occurs at the leading edge of the cells under the two types of cell migration, chemotaxis and wound healing. Time lapse imaging of microtubules marked by enhanced green fluorescent protein-RAPL showed the directional growth of microtubules toward the leading edge of the migrating cells. Using adenovirus, inactivation of Rap1 by expression of rap1GAPII inhibited wound healing. In addition, disconnection of Rap1 and RAPL by expression of a RAPL mutant also perturbed wound healing. Collectively, the locally activated Rap1 and its association with RAPL controls the directional migration of vascular endothelial cells.

Rap1 belongs to the Ras GTPase family and cycles between a GDP-bound inactive form and a GTP-bound active form (1). Rap1 activation is regulated by guanine nucleotide exchange factor (GEF),[1] whereas Rap1 inactivation is regulated by GTPase-activating protein (GAP). GEFs contain a catalytic domain and regulatory domains that either bind to upstream molecules or are regulated by second messengers such as cAMP and Ca^{2+}. The former GEFs include C3G and PDZ-GEF; the latter includes CalDAG-GEFs and Epac (cAMP-GEF) (reviewed in Ref. 2). Thus, the spatial Rap1 activation depends on the localization of GEF and the spreading of second messengers. Like GEFs, the spatial Rap1 inactivation depends on the localization of GAPs for Rap1 (3). We have currently developed a spatio-temporal activation/inactivation monitoring probe for Rap1 in living cells (4).

Once activated by GEFs, GTP-bound Rap1 associates with effector molecules including Raf-1, B-Raf, RalGDS, and AF-6 (2). Rap1 shares these effector molecules with Ras protein; therefore, Rap1 is suggested to function antagonistically on the Ras-activated intracellular signaling pathway. However, Rap1 may have a unique function in regulating cell adhesion (5, 6). Rap1 was recently reported to be indispensable for cell-extracellular matrix (ECM) contacts by stabilizing the cell-ECM contacts, indicating that Rap1 enhances cell adhesion to ECM (7, 8). Moreover, Bud1, the yeast homologue of Rap1, determines the budding site (9), and Rap1 regulates adherens junction positioning for cell division in *Drosophila* (10), implying that Rap1 is also involved in cell polarization.

Cells have a polarity determined by cell protrusions and retractions, when moving toward certain chemoattractants or during wound healing. In the protrusions, actin is actively polymerized and depolymerized, whereas in retractions stabilized actin fibers are observed (11). For perpetual moving toward the chemoattractants, asymmetrical polarity of cell contacts to ECM is required. Focal adhesions connecting actin stress fibers are assembled in the protrusions and disassembled in the retractions of migrating cells (reviewed in Ref. 12). Like actin, microtubules are assembled toward the leading edge of the protrusions. By constituting rails for motor proteins carrying the molecules to the protrusive part of the cell, microtubule promotes cell polarity (13). Furthermore, recently, assembly and disassembly of focal adhesions are reportedly regulated by microtubules (14, 15). Thus, microtubule extension toward the leading edge parallels the change in polarity of the motile cells toward the chemoattractants or during wound healing.

* This work was supported by grants from the Ministry of Health, Labor, and Welfare of Japan; from the Promotion of Fundamental Studies in Health Science of the Organization for Pharmaceutical Safety and Research of Japan; from the Ministry of Education, Science, Sports and Culture of Japan; from the Cell Science Research Foundation; and from the Mochida Memorial Foundation for Medical and Pharmaceutical Research. The costs of publication of this article were defrayed in part by the payment of page charges. This article must therefore be hereby marked "*advertisement*" in accordance with 18 U.S.C. Section 1734 solely to indicate this fact.

[S] The on-line version of this article (available at http://www.jbc.org) contains two additional figures and eight videos.

‡ To whom correspondence should be addressed: Dept. of Structural Analysis, National Cardiovascular Center Research Institute, 5-7-1 Fujishirodai, Suita, Osaka 565-8565, Japan. Tel.: 81-6-6833-5012 (ext. 2508); Fax: 81-6-6835-5461; E-mail: nmochizu@ri.ncvc.go.jp.

[1] The abbreviations used are: GEF, guanine nucleotide exchange factor; CFP, cyan fluorescent protein; ECM, extracellular matrix; EGFP, enhanced green fluorescent protein; FRET, fluorescence resonance energy transfer; GAP, GTPase-activating protein; GFP, green fluorescent protein; GST, glutathione *S*-transferase; HAEC, human aortic endothelial cell; HUVEC, human umbilical vein endothelial cell; MTOC, microtubule-organizing center; Rassf, Ras association domain family; S1P, sphingosine 1-phosphate; SDF-1, stromal-derived factor-1; YFP, yellow fluorescent protein; MES, 4-morpholineethanesulfonic acid.

RAPL/NORE1B (hereafter referred to as RAPL) is identified as a Rap1-binding molecule (16), which contains a Ras/Rap1 binding domain and belongs to the Ras association domain family (Rassf) (17, 18). Whereas Rassf members function as potent suppressors of tumors (19–21), RAPL links Rap1 activation upon T cell receptor cross-linking and stromal-derived factor-1 (SDF-1) stimulation to integrin activation. In addition, RAPL mediates the polarized distribution of SDF-1 receptors upon Rap1 activation (16). Recently, Rassf1 has been shown to localize at and stabilize microtubules (22). However, it is unclear whether other molecules belonging to Rassf function in the association with Ras family GTPases.

We investigate the localization of RAPL in the vascular endothelial cells and how Rap1-RAPL participates in determining the directional migration in response to a chemoattractant, sphingosine 1-phosphate (S1P) (23), and during wound healing. RAPL localizes at the microtubule-organizing center (MTOC) and microtubules. Rap1 is activated at the leading edge of migrating cells. In addition, inactivation of Rap1-RAPL signal perturbed the wound closure. These data suggest that local activation of Rap1 and its association with RAPL regulates the directional cell migration of vascular endothelial cells.

EXPERIMENTAL PROCEDURES

Reagents and Antibodies—S1P was purchased from Biomol (Plymouth, PA). Protein A-Sepharose was from Calbiochem. Anti-green fluorescent protein (GFP) was developed in our laboratory. Anti-β-tubulin, anti-γ-tubulin, and anti-FLAG (M2) were purchased from Sigma, and anti-Rap1 was from BD Biosciences. Anti-RAPL antibody was a kind gift from T. Kinashi (Kyoto University, Japan).

Plasmids—The coding sequences of human Rassf1A, Rassf1C, Rassf2 (KIAA0168), Rassf3, and RAPL (NORE1B) were amplified by PCR using human heart cDNA library as a template. pCA-EGFP-Rassf1A, -Rassf1C, -Rassf2, -Rassf3, and RAPL were derived from pCAGGS eukaryotic expression vector and expressed enhanced green fluorescent protein (EGFP)-tagged each Rassf molecules (24). cDNAs encoding RAPL deletion mutants as indicated in Fig. 4 were amplified by PCR and ligated into pCA-EGFP vector similarly to Rassf1. dC1, dC2, dC3, and dN encoded amino acids 1–222, 1–168, 1–100, and 101–265 of RPAL, respectively. A mutant of RAPL (hereafter referred to as the RA mutant), in which Lys^{123}, Arg^{124}, Lys^{135}, Lys^{154}, Lys^{155}, Asp^{160}, and Asn^{161} were replaced with Ala, was reported to be incapable of associating with Rap1 (16). cDNA encoding an RA mutant was amplified by PCR-based mutagenesis and subcloned into pCA-EGFP. pCXN2-FLAG-Rap1 expressed FLAG-tagged Rap1. Either constitutive active or dominant negative forms of Rap1 (Rap1V12 or Rap1N17) cDNAs were similarly inserted into pCXN2-FLAG. pIRM21-Rap1V12 expressed FLAG-tagged Rap1V12 and internal ribosomal entry site-driven dsFP593 as described previously (24). pIRM21-rap1GAPII expressed both FLAG-tagged rap1GAPII and internal ribosomal entry site-driven dsFP593. pCA-DsRed-CrkI was derived from pCAGGS eukaryotic expression vector as described previously (24). pRaichu-Rap1, a Rap1 activation monitoring probe based on fluorescence resonance energy transfer (FRET), was described previously (4). pRaichu-Rap1 expressed a chimeric protein consisting of yellow fluorescent protein (YFP), Rap1, and Ras-binding domain of Raf and cyan fluorescent protein (CFP) followed by the CAAX motif of Ki-Ras. In pRaichu-Rap1N17, a cDNA encoding Rap1N17 was replaced with that encoding Rap1. pGEX-RAPL was constructed by inserting a cDNA encoding full-length RAPL into pGEX (Amersham Biosciences).

Adenovirus—Both an adenovirus-expressing EGFP-tagged RAPL and an adenovirus-expressing EGFP-tagged RA mutant of RAPL were produced using the Adeno-X expression system (BD Biosciences). Briefly, cDNA from pCA-EGFP-RAPL was inserted into Adeno-X viral DNA using pShuttle as a transfer vector. Adenovirus-expressing EGFP-RAPL was produced from HEK293 cells transfected with Adeno-X-EGFP-RAPL. An adenovirus-expressing RA mutant of RAPL was produced in a similar manner to RAPL-expressing adenovirus. The EGFP-expressing adenovirus and the rap1GAPII-expressing adenovirus were generous gifts from H. Kurose (Kyushu University, Japan) and S. Hattori (Tokyo University, Japan), respectively.

Cell Culture and Transfection—Human umbilical vein endothelial cells (HUVECs) and human aortic endothelial cells (HAECs) were purchased from Cascade Biologics, Inc. (Portland, OR) and cultured in Humedia-EG2 as previously reported (24). HEK293T cells were generous gifts from Dr. B. J. Mayer (University of Connecticut) and maintained as described previously. Jurkat cells and HEK293 cells were obtained from the American Type Culture Collection (Manassas, VA) and cultured in RPMI 1640 (Invitrogen) and Dulbecco's modified Eagle's medium supplemented with 10% fetal bovine serum. Cultured cells were transfected using Lipofectamine 2000 reagent (Invitrogen).

Reverse Transcription-PCR, Pull-down Assay, Immunoprecipitation, and Immunoblotting—RNAs from cultured Jurkat cells and HUVECs were prepared by TRIzol (Invitrogen). cDNAs was synthesized by reverse transcriptase reaction using random primer and RNAs as templates. The cDNA specific for human RAPL was amplified by PCR using a primer set (5'RAPL, CTGGACGAGGAACTGGAAGACTGCTTC; 3'RAPL, AGGGATGGAGAAGGCATCCCACTCTAC). GTP-bound Rap1 was detected according to the method of Bos and co-workers (25). Briefly, HUVECs stimulated with 1 μM S1P for the time indicated at the *top* of Fig. 5 were lysed in lysis buffer (50 mM Tris, pH 7.5, 150 mM NaCl, 5 mM $MgCl_2$, 1% Nonidet P-40, 0.1% SDS, 0.5% deoxycholic acid, 1 mM Na_3VO_4). Precleared lysates were incubated with GST-Rap1-binding domain of RalGDS and glutathione-Sepharose beads. Proteins collected on the beads were subjected to SDS-PAGE followed by immunoblotting with anti-Rap1 antibody. Immunoprecipitation and immunoblotting were performed as described previously (26). Briefly, HEK293T transfected with plasmids as indicated in Fig. 1 were lysed using lysis buffer. Lysates were precleared by centrifugation at 15,000 × *g* for 10 min, followed by immunoprecipitation using anti-GFP and Protein A-Sepharose. Immunoprecipitates were subjected to SDS-PAGE and immunoblotting with anti-FLAG antibody and peroxidase-conjugated goat anti-mouse IgG as a primary and a secondary antibody, respectively. Proteins reacting with anti-FLAG were visualized by an ECL system (Amersham Biosciences) and an LAS-1000 system (Fuji Film, Japan).

Microtubule Binding Assay—Microtubule-associating protein-containing microtubule prepared from bovine brain were gifts from N. Yamagishi (Kyoto Pharmaceutical University, Japan). Glutathione *S*-transferase-fused RAPL (GST-RAPL) expressed in BL21-Star bacteria (Invitrogen) was collected on glutathione-Sepharose (Amersham Biosciences). GST-RAPL was eluted using 10 mM glutathione, precleared by centrifugation at 400,000 × *g*, and polymerized in microtubule-binding buffer (100 mM MES-KOH (pH 6.8), 2 mM EDTA, 1 mM $MgCl_2$, 10 mM Taxol, 4 M glycerol, and 1 mM GTP). For the microtubule binding assay, 5 μg of purified microtubules and GST-RAPL at the concentration indicated in Fig. 3 legend were mixed in 200 μl of microtubule-binding buffer for 30 min at 37 °C. After centrifugation at 400,000 × *g* for 15 min, equal amounts of the supernatant and the pellet were analyzed by SDS-PAGE and immunoblotting with anti-GST. Bovine serum albumin fraction V was used as a negative control for GST-RAPL.

Wound Healing Assay and Responses to Chemoattractant from a Micropipette—HUVECs or HAECs transfected with plasmids indicated in the figures were cultured on 35-mm glass bottom dishes coated with collagen until they reached the monolayer state. The cells were scratched by a regular 20-μl pipette tip along the diameter of the bottom glass. The culture medium remained unchanged during wound healing. Monolayer-cultured HUVECs infected with an adenovirus expressing rap1GAPII, an adenovirus expressing EGFP-RAPL, or an adenovirus expressing the RA mutant of RAPL were scratched and time lapse-imaged. HAECs expressing EGFP-RAPL or those expressing Raichu-Rap1 cultured on glass-bottom dishes coated with collagen were exposed to 1 μM S1P supplied by a micropipette (FemtoJet; Eppendorf Japan).

Fluorescence Microscopy and Confocal Imaging—HUVECs or HAECs transfected with plasmids expressing fluorescence-tagged proteins as indicated in the figure legends were imaged on an Olympus IX-81 inverted microscope. The microscope with a 75-watt xenon arc lamp was equipped with a cooled charge-coupled device camera, CoolSNAP-HQ (Roper Scientific), and two filter exchangers, controlled by MetaMorph 5.0 software (Molecular Devices). The EGFP image and DsRed image were obtained through an XF2043 dichroic filter (Omega) and either a set of an S484/15 excitation filter and an S515/30 emission filter or a set of an S555/25 excitation filter and an S630/60 emission filter, respectively, as reported previously (27). HUVECs transfected with pCA-EGFP-RAPL cultured on a collagen-coated glass-base dish were fixed by 4% paraformaldehyde at room temperature, followed by permeabilization with 0.1% Triton X-100. Permeabilized cells were incubated with anti-β-tubulin or anti-γ-tubulin antibody. Immunopositive reaction was visualized with Alexa 546 goat-anti-mouse IgG (Molecular Probes, Inc., Eugene, OR). Confocal images of EGFP and Alexa 546 were obtained by an Olympus BX50WI microscope controlled by Fluoview. To monitor the cell shape and localization of fluorescence-tagged molecules in living cells, a phase-contrast image and a fluo-

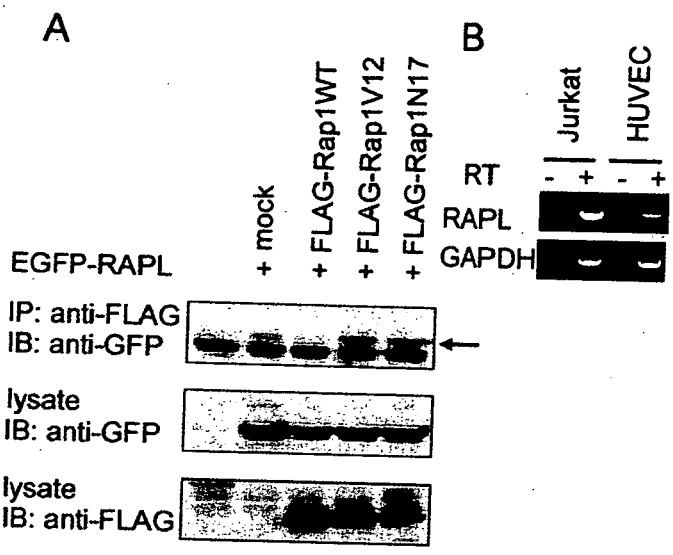

FIG. 1. **The association of RAPL with Rap1 and its expression in vascular endothelial cells.** *A*, HEK293T cells were transfected with plasmids as indicated at the *top*. Cell lysates were subjected to immunoprecipitation (*IP*) followed by immunoblotting (*IB*) with antibodies as indicated on the *left* or directly subjected to SDS-PAGE followed by immunoblotting with the antibodies as indicated on the *left*. An *arrow* denotes GTP-bound Rap1 co-immunoprecipitated with EGFP-tagged RAPL. *B*, RNA prepared from the cells as indicated at the *top* was subjected to reverse transcription-PCR analysis. The sequence of RAPL-specific primers is described under "Experimental Procedures." RNA from Jurkat cells was used as a positive control. The results are representative of more than three independent experiments.

rescence image were obtained every 20 s. A series of time lapse images were converted into video format using MetaMorph 5.0.

Imaging of Rap1 Activation in Living Cells—HAECs cultured on collagen-coated 35-mm diameter glass base dishes were transfected with pRaichu-Rap1 and observed after scratching. Cells similarly transfected with pRaichu-Rap1 were observed during exposure to 1 μM S1P supplied by a micropipette. The structure of Raichu-Rap1 and the principle of FRET is illustrated as in Fig. 5*D*. Cells were imaged on an Olympus IX-81 inverted fluorescence microscope in a method similar to fluorescence imaging as described previously (24). Dual images for CFP and YFP were obtained through an XF1071 excitation filter, an XF2034 dichroic filter, and an XF3075 emission filter for CFP and an XF3079 for YFP (Omega), respectively. The ratio image of YFP/CFP were created by MetaMorph 5.0 software and displayed as an intensity-modulated display image as described previously (4).

RESULTS

A Rap1-binding Protein, RAPL, Is Expressed in Vascular Endothelial Cells—RAPL associates with Rap1 upon T-cell receptor stimulation or chemokine stimulation, resulting in redistribution of integrin in lymphocytes (16). Vascular endothelial cells and hematopoietic cells originate from common hemangioblasts; therefore, we tested whether vascular endothelial cells express RAPL, since Jurkat cells express RAPL (16). RAPL expression was examined by reverse transcription-PCR analysis using a RAPL-specific primer set. HUVECs expressed RAPL mRNA similarly to Jurkat cells used as a positive control (Fig. 1*A*). We further examined the association of GTP-Rap1 with RAPL by the co-immunoprecipitation assay using 293T cells (Fig. 1*B*).

A member of Rassf1A localizes to microtubules in COS cells (22), whereas the localization of RAPL has not yet been clearly demonstrated, although it is reported to accumulate at the leading edge of T lymphocytes (16). Thus, we tested the localization of RAPL in the vascular endothelial cells by using EGFP-tagged RAPL. Rassf members as listed (Fig. 2*A*) were tagged with EGFP and expressed in HAECs. All Rassf members contain the Ras- and Rap1-binding domain (RA domain) (Fig. 2*A*). The expression of EGFP-tagged Rassfs was confirmed by the immunoblot analysis from the lysates of HEK293T cells transfected with the plasmids as indicated at the *top* (Fig. 2*B*). EGFP-tagged Rassf1A and -1C, splicing variants from the same gene, were found as circular fibers in the central region of cells except the nucleus, whereas EGFP-tagged Rassf3 and EGFP-RAPL were found as fibers emanating from the central to the periphery. These results suggested that the circular fibers on which EGFP-tagged Rassf1A and -1C localized may represent microtubules deformed by Rassf1-induced stabilization, as previously demonstrated (22). Rassf3 and RAPL appeared to localize on normal microtubules originating from MTOC to the periphery. Thus, we examined the colocalization of EGFP-RAPL with β-tubulin-constituting microtubules and with γ-tubulin preferably localized on MTOC. As expected, EGFP-RAPL clearly localized on microtubules from the MTOC to the periphery (Fig. 2*D*). In clear contrast to these fibrous expressions, EGFP-Rassf2 was found exclusively in the nucleus. We compared the EGFP-RAPL with EGFP-Rassf1A expressed in motile vascular endothelial cells using time lapse imaging. Both RAPL-expressing cells and Rassf1A-expressing cells showed membrane ruffling (Supplemental Video 1); however, microtubules marked by EGFP-RAPL moved dynamically as regular microtubules, whereas those marked by EGFP-Rassf1 were static (Supplemental Video 2). These data indicated that Rassf members, Rassf3 and RAPL, appear to bind to microtubules without affecting the endogenous microtubule structure.

We further confirmed the localization of RAPL on microtubules by immunostaining using anti-RAPL antibody. Endogenous RAPL localized on microtubules in HAECs (Fig. 3*A*). The association of RAPL and microtubules were examined by biochemical analysis using purified microtubules and GST-RAPL. The microtubule binding assay revealed that GST-RAPL cosedimented with microtubules in a concentration-dependent manner. Although GST-RAPL and tubulin closely migrated in SDS-PAGE (Fig. 3*B*, *top panel*), GST-RAPL was clearly separated by immunoblotting with anti-GST (Fig. 3*B*, *middle panel*). In agreement with these observations, when microtubule formation was inhibited by nocodazole, the filamentous expression of RAPL was not observed (Supplemental Fig. 1). Collectively, these results indicated that endogenous RAPL localizes on microtubules in vascular endothelial cells.

RAPL Requires Rap1-associating Domain for Localizing on Microtubules but Not Its Association with Rap1—To define the region responsible for the association of RAPL with microtubules, we constructed a series of truncated mutants and a mutant incapable of associating with Rap1 (RA mutant) (Fig. 4*A*). The expression of EGFP-tagged RAPL and its mutants was confirmed by the immunoblot analysis from the lysates of HEK293T cells transfected with the plasmids as indicated at the *top* of Fig. 4*B*. We examined the expression of EGFP-tagged RAPL and its mutants in HAECs (Fig. 4*C*). EGFP-tagged full-length RAPL and coiled-coil domain-lacking mutant (dC1) localized on microtubules. Intriguingly, RA mutant also localized on microtubules. However, neither RA domain-lacking mutant (dC2 and dC3) nor a mutant lacking the amino-terminal 100 amino acids (dN) localized on microtubules. The EGFP-tagged RA domain alone was not expressed on the microtubules. These data indicated that the association of RAPL with Rap1 is not required for the localization of RAPL on microtubules and that the amino-terminal part of RAPL and the RA domain are essential for its targeting to microtubules.

Rap1 Locally Activated by S1P Triggers Directional Migration Preceding Microtubule Extension—To understand the significance of Rap1 activation and RAPL localizing on microtubules, we examined RAPL localization in HAECs expressing either Rap1V12 or rap1GAPII. EGFP-RAPL dislocated from microtu-